Integration of a Notch-dependent mesenchymal gene program and Bmp2-driven cell invasiveness regulates murine cardiac valve formation

Luis Luna-Zurita,[1] Belén Prados,[1] Joaquim Grego-Bessa,[1] Guillermo Luxán,[1] Gonzalo del Monte,[1] Alberto Benguría,[1] Ralf H. Adams,[2] José María Pérez-Pomares,[3] and José Luis de la Pompa[1]

[1]Laboratorio de Biología Celular y del Desarrollo, Departamento de Biología del Desarrollo Cardiovascular, Centro Nacional de Investigaciones Cardiovasculares (CNIC), Madrid, Spain.
[2]Max-Planck-Institute for Molecular Biomedicine and University of Münster, Faculty of Medicine, Münster, Germany.
[3]Departamento de Biología Animal, Facultad de Ciencias, Universidad de Málaga, Málaga, Spain.

Cardiac valve formation is crucial for embryonic and adult heart function. Valve malformations constitute the most common congenital cardiac defect, but little is known about the molecular mechanisms regulating valve formation and homeostasis. Here, we show that endocardial Notch1 and myocardial Bmp2 signal integration establish a valve-forming field between 2 chamber developmental domains. Patterning occurs through the activation of endocardial epithelial-to-mesenchymal transition (EMT) exclusively in prospective valve territories. Mice with constitutive endocardial Notch1 activity ectopically express *Hey1* and *Heyl*. They also display an activated mesenchymal gene program in ventricles and a partial (noninvasive) EMT in vitro that becomes invasive upon BMP2 treatment. *Snail1*, TGF-β2, or Notch1 inhibition reduces BMP2-induced ventricular transformation and invasion, whereas BMP2 treatment inhibits endothelial Gsk3β, stabilizing Snail1 and promoting invasiveness. Integration of Notch and Bmp2 signals is consistent with Notch1 signaling being attenuated after myocardial *Bmp2* deletion. Notch1 activation in myocardium extends *Hey1* expression to nonchamber myocardium, represses *Bmp2*, and impairs EMT. In contrast, Notch deletion abrogates endocardial *Hey* gene transcription and extends *Bmp2* expression to the ventricular endocardium. This embryonic Notch1-Bmp2-Snail1 relationship may be relevant in adult valve disease, in which decreased NOTCH signaling causes valve mesenchyme cell formation, fibrosis, and calcification.

Introduction

Congenital cardiac valvuloseptal defects are the most frequently diagnosed developmental malformations during the first year of human life (1), and several valvular defects manifest in adult disease (2). Evidence from animal models has linked many genes and signaling pathways to cardiac valve development (3); however, mutations of the human homologs seldom correlate with human valve defects (4). Moreover, the similar phenotypes of targeted mutant mice suggest they affect functionally interconnected signaling pathways (5).

Cardiac valve formation (CVF) in mice begins at approximately E9.5. In the developing atrioventricular canal (AVC) and outflow tract (OFT), myocardial signals induce adjacent endocardial cells (ENCs) to undergo epithelial-to-mesenchymal transition (EMT) (5). These cells invade the underlying matrix (cardiac jelly) to generate the heart valve primordia (endocardial cushions). Cardiac EMT begins with ENC activation, in which ENCs swell due to the enlargement of the Golgi and rough endoplasmic reticulum. Transformation follows, in which ENCs lose cell: cell contacts, acquire the ability to move into the plane of the monolayer, polarize their Golgi, and form migratory appendages. EMT is completed once the transformed ENCs invade the cardiac jelly to form the valvuloseptal mesenchyme (6). ENC transformation is dependent on the initiation of EMT-specific transcriptional machinery, the physical detachment of epithelial cells, and the activation and stabilization of a migratory and invasive mesenchymal phenotype.

Defining the primary signal or signals inducing cardiac EMT has been problematic due to the difficulties of extrapolating results from chick and mouse (5) and because the exact extent of spatiotemporal interaction between myocardium and endocardium cannot be fully reproduced in vitro. Data from collagen gel assays with chicken tissue suggested TGF-β2 or TGF-β3 as the main myocardial EMT inducers (7); however, *Tgfb2*- or *Tgfb3*-deficient mice show no endocardial EMT defect, suggesting induction of mammalian EMT by other signals (8). Indeed, in mice, Bmp2 is critical for EMT induction in vitro (9) and in vivo (10) and Bmp2 alone can specify a field of cardiac progenitors as a heart valve–inducing region (11).

Within the endocardium, EMT is regulated by Notch (12), an ancient local cell signaling system in which both ligands (Delta and Jagged) and receptors (Notch) are membrane bound (13). Ligand-receptor binding initiates 2 consecutive receptor cleavage steps, the last one involving γ-secretase (13), to generate the biologically active Notch intracellular domain (NICD). In the nucleus, NICD binds the RBPJK/CSL transcription factor and regulates target gene expression and thus cell fate specification (13). Notch1 activity delineates AVC and OFT endocardium in the mouse E9.5 heart (14), and the AVC of *RBPJk*- and *Notch1*-targeted mutants almost completely lacks mesenchymal cushion cells (12). Although

Conflict of interest: The authors have declared that no conflict of interest exists.
Citation for this article: *J Clin Invest.* 2010;120(10):3493–3507. doi:10.1172/JCI42666.

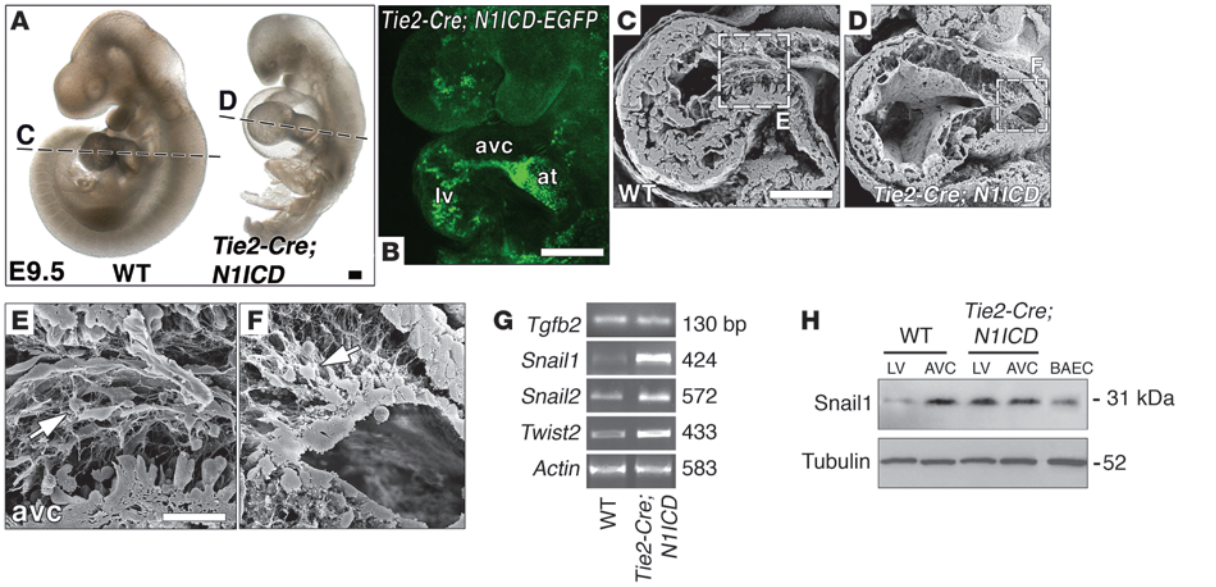
A
C
D
E9.5
WT
Tie2-Cre;
N1ICD
Tie2-Cre; N1ICD-EGFP
avc
at
lv
B
C
E
WT
D
F
Tie2-Cre; N1ICD
E
F
avc
G
Tgfb2
Snail1
Snail2
Twist2
Actin
130 bp
424
572
433
583
WT
Tie2-Cre; N1ICD
H
WT
Tie2-Cre; N1ICD
LV
AVC
LV
AVC
BAEC
Snail1
- 31 kDa
Tubulin
-52

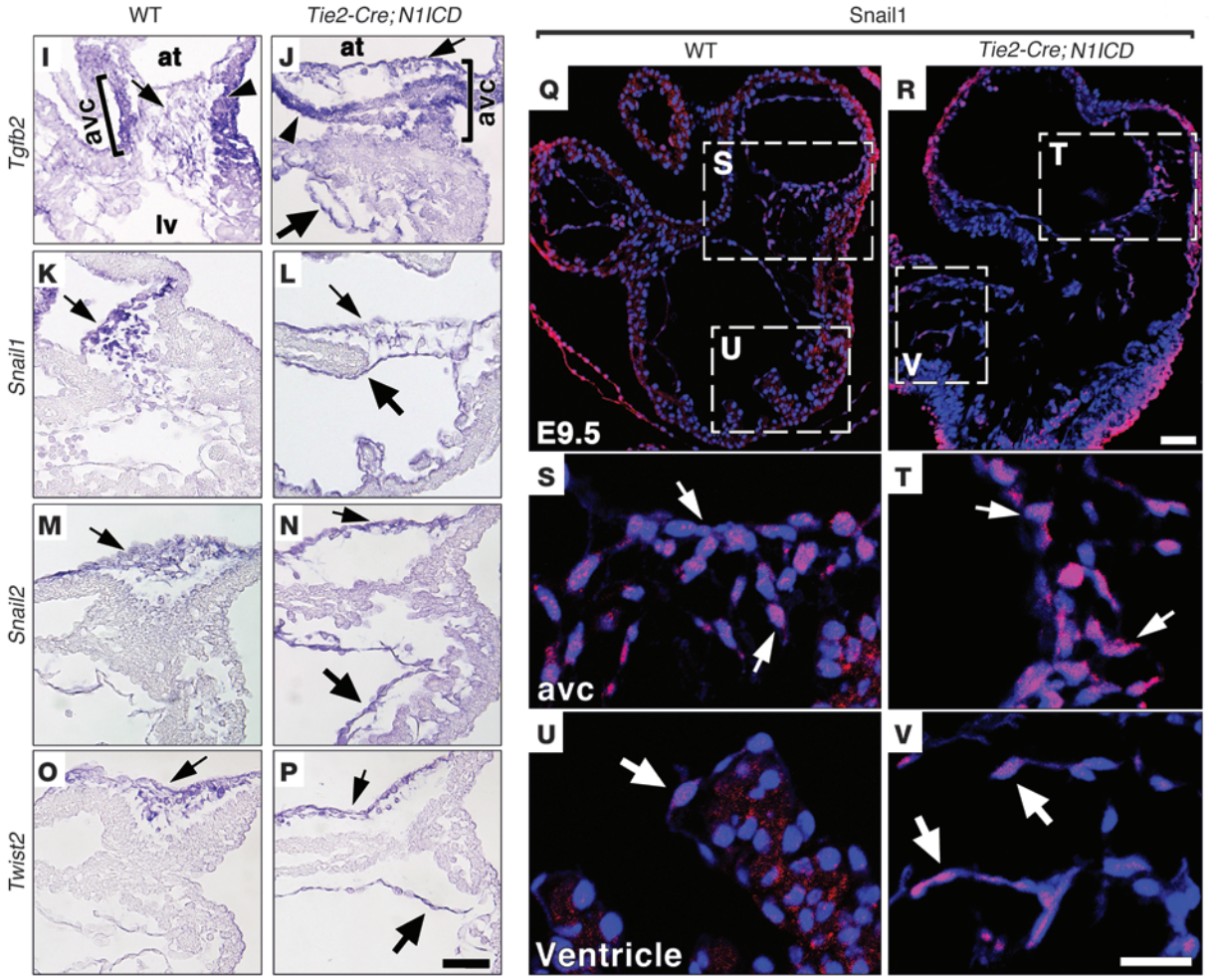
WT
Tie2-Cre; N1ICD
Snail1
WT
Tie2-Cre; N1ICD
Tgfb2
Snail1
Snail2
Twist2
I
at
avc
lv
J
at
avc
K
L
M
N
O
P
Q
S
U
E9.5
R
T
V
S
avc
T
U
Ventricle
V

Figure 1
E9.5 *Tie2-Cre;N1ICD* mice ectopically express mesenchyme genes in chamber endocardium. (**A**) WT and *Tie2-Cre;N1ICD* embryos. Dotted lines indicate **C** and **D** section planes. (**B**) Endocardial EGFP expression in a *Tie2-Cre;N1ICD* embryo. at, atrium. (**C** and **D**) SEM images of longitudinal WT (**C**) and *Tie2-Cre;N1ICD* (**D**) heart sections. (**E** and **F**) Details of AVC in WT (**E**) and *Tie2-Cre;N1ICD* hearts (**F**). Arrows, mesenchymal cells. (**G**) Semiquantitative RT-PCR analysis in hearts. (**H**) Snail1 Western blot. (**I**–**P**) WISH, heart details. Arrowheads, AVC myocardium; thin arrows, AVC endocardium; thick arrows, ventricular endocardium. (**I**) *Tgfb2* expression in WT AVC myocardium and endocardium (bracket). (**J**) Normal *Tgfb2* expression in AVC and ectopic expression in ventricular endocardium of *Tie2-Cre;N1ICD* embryos. (**K** and **L**) WT mice express *Snail1* in AVC endocardium and mesenchyme (**K**); *Tie2-Cre;N1ICD* embryos show ectopic expression in ventricular endocardium (**L**). *Tie2-Cre;N1ICD* hearts also show ectopic ventricular expression of *Snail2* (**N**) and *Twist2* (**P**). (**Q**–**V**) Snail1 expression (red) in E9.5 heart. Nuclei are DAPI counterstained (blue). (**Q**) General view of an E9.5 WT heart. (**S**) Detail of AVC region. Arrows, nuclear Snail1 in endocardial and mesenchyme cells. (**U**) Detail of LV region with an ENC weakly expressing Snail1 (arrow). (**R**) General view of *Tie2-Cre;N1ICD* heart. (**T**) Detail of AVC. Arrows, nuclear Snail1 staining in endocardium and mesenchyme. (**V**) Ectopic Snail1 staining in ventricular endocardium. Scale bars: 100 μm (**A** and **B**); 125 μm (**C** and **D**); 20 μm (**E** and **F**); 10 μm (**I**–**P**); 30 μm (**Q** and **R**); 20 μm (**S**–**V**).

ENCs from E9.5 *RBPJk*-deficient AVC show some features of activated premigratory endocardium, they remain in close association, maintain adherens junctions, and fail to invade the cardiac jelly. This correlates with reduced transcription of the cadherin repressor Snail1, which is normally expressed in AVC and OFT endocardium and mesenchyme (12). Loss of *Snail1* expression thus appears to block EMT by preventing downregulation of ENC cell adhesion. *RBPJk* and *Notch1* mutant AVC explants cultured on collagen gels fail to undergo EMT, a finding confirmed by Notch inhibition in WT mouse AVC explants and zebrafish embryos (12). Moreover, deletion of the Notch target *Hey2* produces AV valve defects (15), and double *Hey1;Hey2* or *Hey1;Heyl* mutants additionally show severe cardiac EMT defects (16, 17).

Recent data have suggested that *N1ICD* overexpression in zebrafish AVC endocardium inhibits EMT (18), while on the other hand, *Mesp1-Cre* driven *N1ICD* activation in the mouse cardiac lineage impairs AVC myocardial differentiation without affecting EMT (19). These apparently inconsistent data indicate that the precise role of Notch in the regulation of endocardial EMT, its downstream molecular mechanism, and relationship with other activators of this process (e.g., TGF-βs and Bmps) remain to be defined.

Using a variety of mouse genetic models, in vitro assays, and molecular studies, we show that Notch1 is sufficient to activate a cell-autonomous, promesenchymal gene expression program in ENCs. Constitutive Notch1 activity in endocardium enables ectopic, noninvasive EMT of ventricular ENCs, conferring "valvular" features to an otherwise "nonvalvular," EMT-refractory ventricular endocardium. BMP2 treatment of these ventricular ENCs drives EMT to completion by promoting Notch- and Snail1-dependent invasion. Ectopic myocardial *Notch1* expression and loss-of-function experiments indicate that Notch1 represses *Bmp2* in cardiac cells by *Hey* target activation. *Bmp2* inactivation in the myocardium impairs Notch1 activity, suggesting a functional link between these 2 signaling pathways. *Snail1* expression induced by Notch1 and Bmp2 and Snail1 protein stabilization mediated by Bmp2 via Gsk3β inhibition suggest that Notch1 and Bmp2 signals converge to promote ENC invasiveness. We propose a model in which the interplay between myocardial Bmp2 and endocardial Notch1 restricts EMT to prospective valve territory. In this setting, the prevalvular endocardium is not a passive tissue, simply responding to inductive myocardial signals, but plays an active role in promoting EMT.

Results

Endocardial Notch1 activation causes heart dysmorphogenesis and ectopic target gene expression. To investigate whether ectopic Notch1 activation in the heart was sufficient to drive EMT, we activated Notch1 in the endocardium, myocardium, or both tissues. We used the conditional *N1ICD* transgenic line *R26N1ICD*, which upon Cre activation expresses the Notch1 intracellular domain (amino acids 1749–2293) and nuclear-localized enhanced GFP (20). *R26N1ICD* mice (from now on, *N1ICD*) were crossed with the endothelium/endocardium-specific *Tie2-Cre* driver line (ref. 21 and Supplemental Figure 1A; supplemental material available online with this article; doi:10.1172/JCI42666DS1). At E9.5, *Tie2-Cre;N1ICD* embryos were smaller than WT littermates and showed pericardial distension and enlarged LV and atrium (Figure 1A). EGFP expression delineated the endocardium, indicating N1ICD expression (Figure 1B). Scanning electron microscopy revealed AVC mesenchymal cells invading the cushion region in E9.5 WT embryos (Figure 1, C and E). Transgenic littermates had relatively fewer mesenchymal cells in AVC cushion tissue (Figure 1, D and F), probably due to a slight developmental delay. H&E-stained sections were consistent with these findings (Supplemental Figure 1, B–E) and revealed poorly formed trabeculae in E9.5 transgenic embryos (Supplemental Figure 1, F and G).

Whole-mount in situ hybridization (WISH) and RT-PCR in *Tie2-Cre;N1ICD* embryos showed that endocardial expression of *N1ICD* and its targets *Hey1* and *Hey2* (22), *Heyl* (17), *Delta-like 4* (23), *Nrarp* (24), and *c-myc* (25) was increased and expanded from the AVC to the ventricles (Supplemental Figure 1, H–T), indicating increased Notch activity throughout the endocardium. CD31/PECAM and MLC2v expression, indicative of early endocardial and myocardial differentiation, were normal (Supplemental Figure 2 and data not shown). The expression domains of *Anf* (26) and *Chisel* (27) in the AVC were less well defined in *Tie2-Cre;N1ICD* embryos compared with WT animals (Supplemental Figure 2, A and B), though their expression levels were unaffected (Supplemental Figure 2K and data not shown). *Irx5*, normally expressed in ventricular endocardium (ref. 28 and Supplemental Figure 2C), was strongly reduced in *Tie2-Cre;N1ICD* embryos (Supplemental Figure 2, D and K), suggesting loss of chamber identity.

The expression of endothelial identity markers was examined, given that the *Tie2-Cre* driver is active in the vascular endothelium as well (21). *Tie2-Cre;N1ICD* embryos ectopically expressed the *Dll4* and *Efnb2* markers in veins (Supplemental Figure 3, A–D), while expression of the venous marker *Ephb4* was reduced (Supplemental Figure 3, E and F), suggesting that the vascular endothelium of transgenic embryos had lost its venous identity. *Tie2-Cre;N1ICD* embryos died at E11.0, probably as a consequence of defective vascular and hematopoietic development (P. Melgar and J.L. de la Pompa, unpublished observations).

Activation of a mesenchyme gene expression program characteristic of AVC in the ventricular endocardium of Tie2-Cre;N1ICD embryos. Bmp2 is expressed in AVC myocardium at E9.5 and triggers the EMT of adjacent ENCs (9). Bmp2 expression was slightly weaker at E9.5 and was unaffected in E10.5 *Tie2-Cre;N1ICD* embryos (Supple-

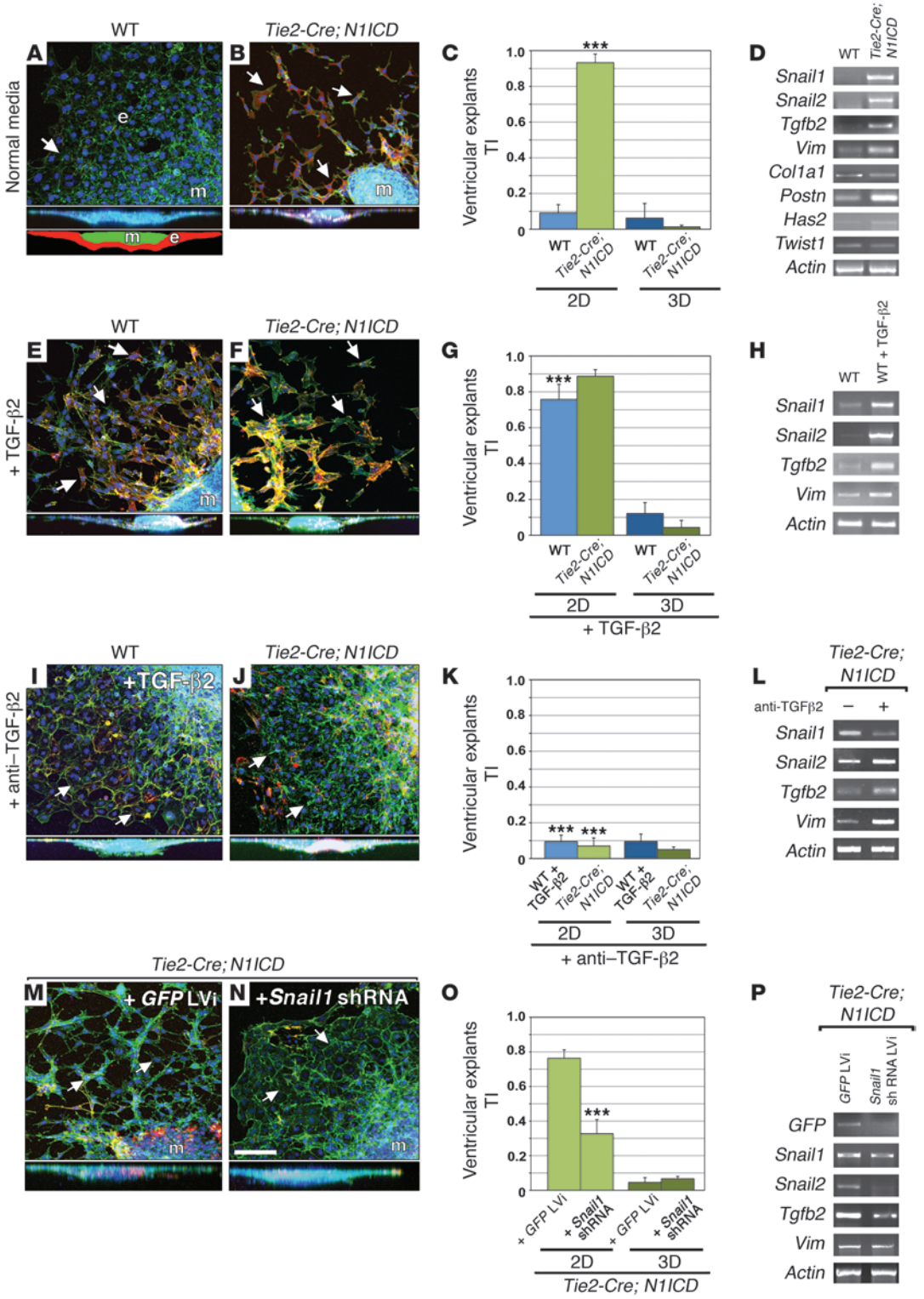
WT
Tie2-Cre; N1ICD
A
B
Normal media
e
m
m
e
C
Ventricular explants
TI
***
1.0
0.8
0.6
0.4
0.2
0
WT
Tie2-Cre; N1ICD
WT
Tie2-Cre; N1ICD
2D
3D
D
WT
Tie2-Cre; N1ICD
Snail1
Snail2
Tgfb2
Vim
Col1a1
Postn
Has2
Twist1
Actin
WT
Tie2-Cre; N1ICD
E
F
+ TGF-β2
m
G
Ventricular explants
TI
***
1.0
0.8
0.6
0.4
0.2
0
WT
Tie2-Cre; N1ICD
WT
Tie2-Cre; N1ICD
2D
3D
+ TGF-β2
H
WT
WT + TGF-β2
Snail1
Snail2
Tgfb2
Vim
Actin
WT
Tie2-Cre; N1ICD
I
+TGF-β2
J
+ anti–TGF-β2
K
Ventricular explants
TI
***
***
1.0
0.8
0.6
0.4
0.2
0
WT + TGF-β2
Tie2-Cre; N1ICD
WT + TGF-β2
Tie2-Cre; N1ICD
2D
3D
+ anti–TGF-β2
L
Tie2-Cre; N1ICD
anti-TGFβ2
–
+
Snail1
Snail2
Tgfb2
Vim
Actin
Tie2-Cre; N1ICD
M
+ GFP LVi
N
+Snail1 shRNA
m
m
O
Ventricular explants
TI
***
1.0
0.8
0.6
0.4
0.2
0
+ GFP LVi
+ Snail1 shRNA
+ GFP LVi
+ Snail1 shRNA
2D
3D
Tie2-Cre; N1ICD
P
Tie2-Cre; N1ICD
GFP LVi
Snail1 sh RNA LVi
GFP
Snail1
Snail2
Tgfb2
Vim
Actin

Figure 2

Tie2-Cre;N1ICD ventricular explants undergo Tgf-β2– and Snail1-mediated ectopic EMT. (**A**, **E**, and **I**) Details of WT explants. (**B**, **F**, **J**, **M**, and **N**) Details of *Tie2-Cre;N1ICD* explants. Full lateral views of explants are shown below panels **A**–**N**. Schematic of a full lateral view of explant is shown at the bottom of panel **A**. e, endocardium (red); m, myocardium (green). All explants were stained with phalloidin-FITC (green), anti–α-SMA–Cy3 (red), and DAPI (blue). Arrows mark ENCs. (**C**, **G**, **K**, and **O**) Quantitative analysis of 2D and 3D TI. (**D**, **H**, **L**, and **P**) RT-PCR of explant endocardium. (**A**) WT. Arrow, ENCs growing as a monolayer. The lateral section shows ENC outgrowth on the collagen surface. (**B**) *Tie2-Cre;N1ICD*. Arrows, scattered ENCs that have undergone partial EMT. (**C**) 2D TI is increased in *Tie2-Cre;N1ICD* explants ($P = 3.7 \times 10^{-4}$). (**D**) *Snail1*, *Snail2*, *Tgfb2*, *Vimentin*, and *Periostin* expression is upregulated; *Has2* is slightly increased and *Twist1* appears unaffected. (**E**, **F**, and **G**) ENCs scatter without invading the collagen in TGF-β2–treated WT explants, and 2D TI is increased with respect to untreated WT ones (**C**; $P = 1.8 \times 10^{-7}$) and *Tie2-Cre;N1ICD* explants. (**H**) Increased *Snail1*, *Snail2*, and *Tgfb2* expression. (**I** and **K**) ENCs of WT explants cultured with TGF-β2 and anti–TGF-β2 antibody grow as a monolayer and show reduced 2D TI with respect to TGF-β2–treated WT (**G**; $P = 8.1 \times 10^{-6}$). (**J** and **K**) Anti–TGF-β2 reduces ENC migration in *Tie2-Cre;N1ICD* explants, reflected in a reduced 2D TI ($P = 2.3 \times 10^{-5}$) and attenuated *Snail1* expression (**L**). (**M**–**O**) Lentiviral-mediated *shRNA Snail1* downregulation in transgenic explants reduces ENC migration with respect to GFP-transduced control explants ($P = 3.3 \times 10^{-8}$). LVi, lentivirus. (**P**) Expression of *Snail2* and *Tgfb2* is reduced. Scale bar: 50 μm. Results are expressed as mean + SD. ***$P < 0.001$.

mental Figure 2, E, F, and K). Tgf-β2, which acts downstream of Bmp2 (9) is transcribed in AVC myocardium at E9.5 and at lower levels in AVC endocardium and mesenchyme (ref. 8, Figure 1I, and Supplemental Figure 5A). *Tgfb2* showed slightly weaker expression in *Tie2-Cre;N1ICD* AVC and was ectopically expressed in ventricular endocardium (Figure 1J and Supplemental Figure 5B). RT-PCR revealed normal *Tgfb2* expression, probably because of ectopic expression in the ventricles (Figure 1G). *Snail1*, expressed in response to Notch (12) and TGF-β2 (29), was detected in AVC endocardium and mesenchymal cells of WT embryos (Figure 1K and Supplemental Figure 5C). In transgenic embryos, *Snail1* transcription was extended to the ventricular endocardium (Figure 1L and Supplemental Figure 5D) and increased (Figure 1G). Ectopic Snail1 expression in ventricles was confirmed by Western blot (Figure 1H). Immunostaining showed Snail1 expression in the nuclei of WT and *Tie2-Cre;N1ICD* AVC endocardial and mesenchyme cells (Figure 1, Q–T). Transgenic embryos displayed ectopic nuclear Snail1 expression in ventricular ENCs (Figure 1, U and V). Sox9, a Tgf-β2 target in mesenchymal cells implicated in endocardial cushion cell differentiation (30), was transcribed in AVC endocardium and mesenchyme (Supplemental Figure 4A) and its expression was increased and expanded to the ventricles in transgenic embryos (Supplemental Figure 4, B and I).

Affymetrix microarray analysis to identify additional genes differentially expressed in *Tie2-Cre;N1ICD* E9.5 hearts uncovered 516 genes, 66 of which were downregulated and 450 of which were upregulated (Supplemental Excel file). Many of the upregulated genes were associated with EMT initiation, mesenchymal phenotype maintenance, cell migration, invasion, adhesion, and collagen deposition (Supplemental Table 1). These included *Snail2*, *Twist2*, *Bmp6*, and the Bmp receptor genes *Alk3* and *Alk6* (Supplemental Table 1), all of which are essential for EMT in different cellular contexts (31–33). Snail2, like Snail1, is required for Notch-induced EMT (31), and its expression was expanded in *Tie2-Cre;N1ICD* embryos from AVC endocardium and mesenchyme to the ventricular endocardium (Figure 1, M and N, and Supplemental Figure 5, E and F) and increased (Figure 1G). Twist1 is required downstream of Bmp2 during AVC EMT (10), but *Twist1* expression was not altered in the microarray (Supplemental Excel file) or by WISH or RT-PCR (Supplemental Figure 2, G, H, and K), suggesting that Bmp2-dependent signaling in *Tie2-Cre;N1ICD* embryos was unaltered. In contrast, *Twist2* expression was expanded from AVC to ventricles (Figure 1, O and P, and Supplemental Figure 5, G and H) and increased (Figure 1G), but the late EMT marker *Has2* (34) was unaltered (Supplemental Figure 2, I–K). Similarly, *Bmp6*, normally expressed in AVC endocardium (Supplemental Figure 4E) and required for cushion morphogenesis (33), was ectopically expressed in the ventricle of transgenic embryos (Supplemental Figure 4, F and I). Expression of the chemokine receptor gene *Cxcr4*, involved in cell migration and metastasis (35), was increased in transgenic embryos (Supplemental Table 1 and Supplemental Figure 4I) and expanded from AVC endocardium to ventricular endocardium (Supplemental Figure 4, G and H). A further 12 genes involved in EMT, cell migration, and invasion were significantly increased in transgenic embryos (Supplemental Table 1), and upregulation of the Notch pathway genes detected by WISH and RT-PCR (Supplemental Figure 1, H–T) was also confirmed. Thus, *Tie2-Cre;N1ICD* embryos show the expansion of mesenchymal gene expression from AVC to ventricles. Moreover, expression of the chamber marker *Hand2* was strongly reduced (Supplemental Table 1), confirming the loss of ventricular chamber identity in *Tie2-Cre;N1ICD* embryos.

Tie2-Cre;N1ICD ventricular explants undergo Tgf-β2 and Snail1-dependent EMT. Culture of AVC explants on a type I collagen gel lattice is an excellent functional assay to evaluate EMT (36). To quantify differences between WT and transgenic explants, we determined the "transformation index" (TI) in 2 and 3 dimensions. 2D TI is the fraction of ENCs able to detach and migrate on the gel surface without invading the collagen matrix. 3D TI is the fraction able to invade the gel. After 72 hours, E9.5 WT AVC explants produced a halo of mesenchymal cells around the myocardium (Supplemental Figure 6A), with mesenchymal cells invading the collagen depths (Supplemental Figure 6A and Supplemental Video 1). E9.5 *Tie2-Cre;N1ICD* explants also produced invasive mesenchymal cells (Supplemental Figure 6B and Supplemental Video 1), but while 3D TI was similar for both genotypes (3D = 0.1), 2D TI was 3-fold higher in transgenic explants (0.35 vs. 0.15; Supplemental Figure 6C). Expression of EMT-inducing molecules in WT and transgenic ENCs was similar. Similar to the situation in vivo, *Hey1* was ectopically expressed and upregulated in transgenic ENCs, together with *Hey2*, *Heyl*, and the mesenchymal marker *Vimentin* (Supplemental Figure 6D).

To determine whether ectopic Notch1 activity conferred transforming ability on ventricular tissue, we performed explant cultures with the distal tip of the LV. WT explants generated an endocardial monolayer surrounding the myocardium (Figure 2A), and ENCs grew as a coherent epithelium on the collagen surface (Figure 2A and Supplemental Video 2). In contrast, in *Tie2-Cre;N1ICD* explants, ENCs migrated over the gel and had a mesenchymal phenotype revealed by α-SMA staining (Figure 2B). These transformed cells did not invade the collagen matrix (Figure 2B and Supplemental Video 2), but their migratory ability was reflected in a sharply increased 2D TI (0.9 vs. 0.1; Figure 2C). Unlike WT cells,

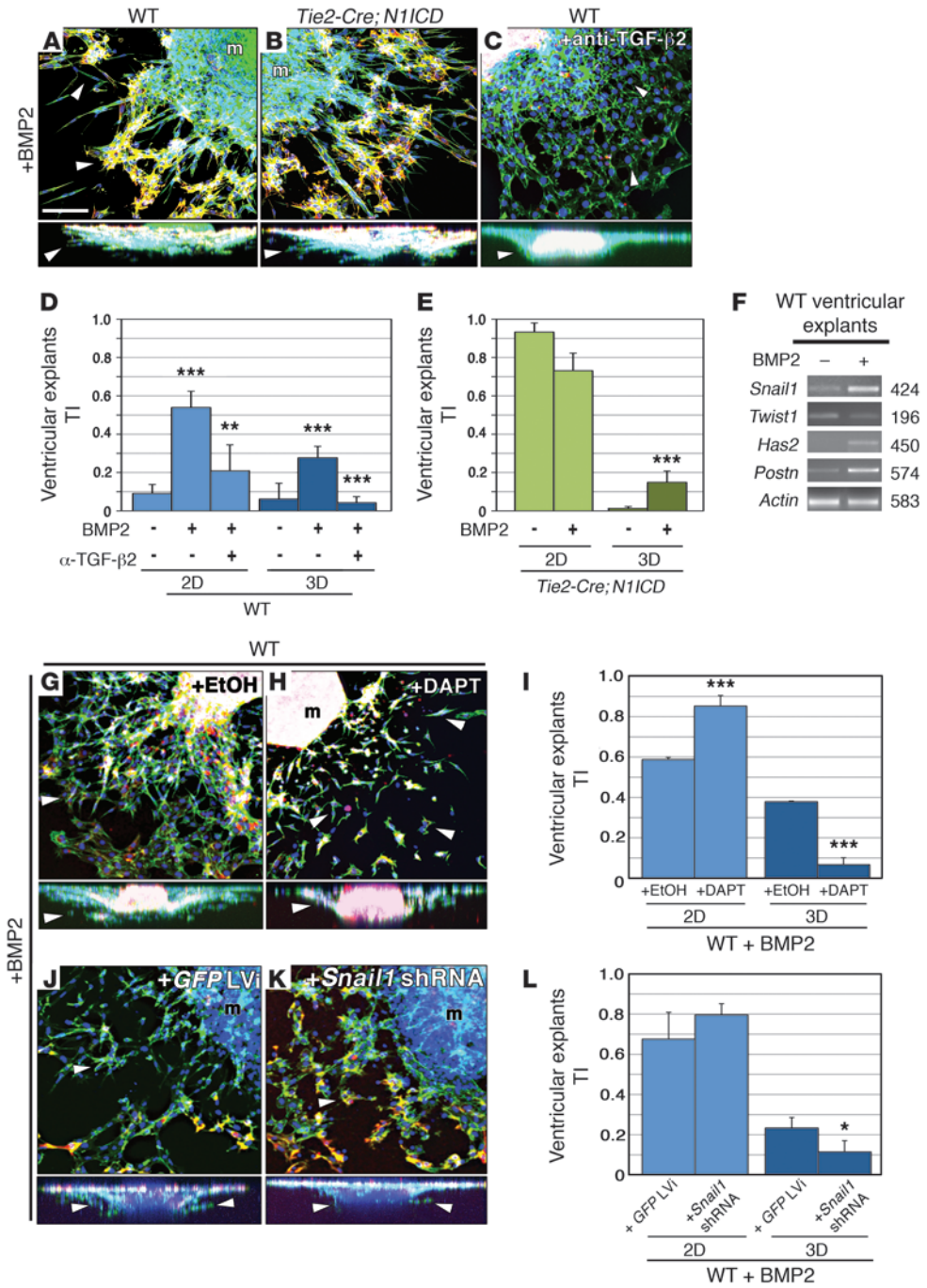

Figure 3

BMP2 induces ventricular explants to undergo Tgf-β2–, Notch-, and Snail1-mediated invasive EMT. All explants were triple stained as in Figure 2. (**A**–**C**, **G**, **H**, **J**, and **K**) Details of explants. Full lateral views are shown below. Arrowheads mark invading ENCs. (**A** and **D**) BMP2 treatment of WT ventricular explants induces invasive EMT, increasing 2D and 3D TI ($P = 2 \times 10^{-4}$ and 2.7×10^{-4}). (**B** and **E**) BMP2 treatment increases the 3D TI of *Tie2-Cre;N1ICD* explants ($P = 9 \times 10^{-4}$) at the expense of reduced 2D TI. (**C** and **D**) Anti–TGF-β2 reduces the 2D and 3D TI of BMP2-treated WT explants ($P = 4.1 \times 10^{-3}$ and 1.8×10^{-7}). (**F**) BMP2-treated WT ventricular explants upregulate *Snail1*, *Has2*, and *Periostin*, but *Twist1* appears unaffected. (**G**–**I**) Inhibition of Notch with DAPT reduces invasive capacity (3D TI) of BMP2-treated WT ventricular explants ($P = 1.02 \times 10^{-8}$), while increasing 2D TI ($P = 1.3 \times 10^{-4}$). (**J**–**L**) Lentiviral-mediated *shRNA Snail1* downregulation reduces the invasive capacity of BMP2-treated WT explants. ($P = 3.4 \times 10^{-2}$). m, myocardium. Scale bar: 50 μm. Results are expressed as mean + SD. $^{**}P < 0.01$; $^{***}P < 0.001$.

ENCs of transgenic explants expressed the mesenchymal markers *Snail1*, *Snail2*, *Tgfb2*, *Vimentin*, *Periostin* (37), and very low levels of *Has2* (ref. 34 and Figure 2D) and *Collagen*. *Twist1* was unaffected, consistent with the in vivo data (Figure 2D).

The transformed ventricular ENCs of *Tie2-Cre;N1ICD* explants showed increased expression of *Tgfb2* (Figure 2D), a key EMT inducer in AVC cells (8). Addition of TGF-β2 to WT ventricular explants mimicked the results with *Tie2-Cre;N1ICD* explants, inducing surface migration of ENCs but not invasion (Figure 2E). TGF-β2–treated WT ventricular explants had a 2D TI similar to untreated transgenic explants (0.75 vs. 0.9; Figure 2G) and expressed *Snail1*, *Snail2*, and *Vimentin* (Figure 2H). TGF-β2 had no additive effect on *Tie2-Cre;N1ICD* explants (Figure 2, F and G). A neutralizing anti–TGF-β2 antibody reverted the phenotype of *Tie2-Cre;N1ICD* and TGF-β2–treated WT ventricular explants to the endocardial monolayer seen in untreated WT explants (Figure 2, I–K), accompanied by reduced mesenchymal marker expression (Figure 2L).

During AVC EMT, Snail1, and Snail2 are key downstream effectors of Notch (12, 31) and TGF-β2 (38). To test the role of the *Snail* genes in the acquisition of the mesenchymal phenotype by ventricular ENCs, we transduced ventricular explant

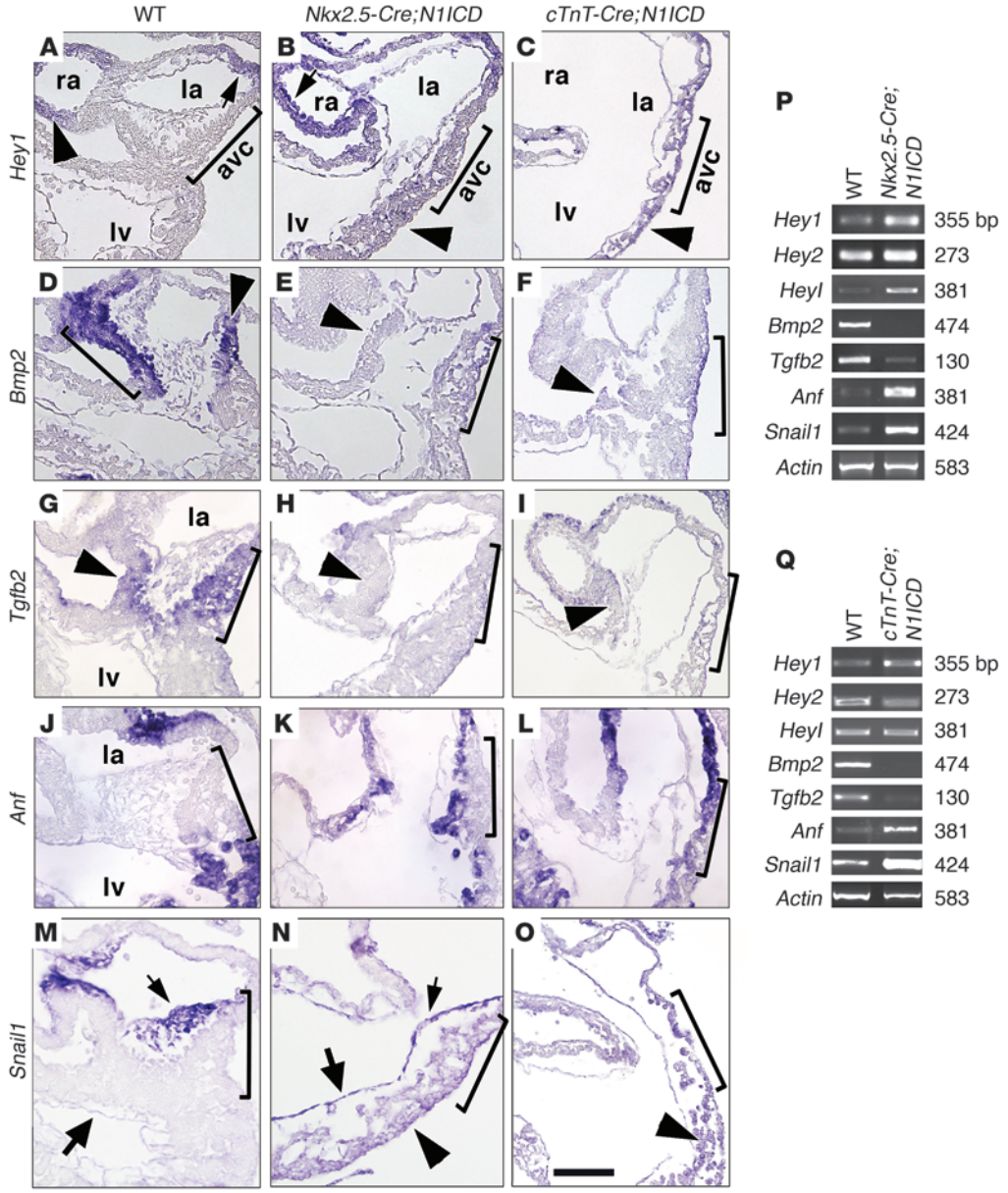

Figure 4
Myocardial Notch1 activation leads to loss of AVC identity. (**A**–**O**) WISH of E9.5 hearts, showing detail of AVC and LV. Brackets mark the AVC. Arrowheads, myocardium; arrows, endocardium. la, left atrium; ra, right atrium. (**A**–**C**) *Hey1*. Expression is restricted to atrial myocardium and endocardium in WT hearts, extends throughout myocardium and endocardium of *Nkx2.5-Cre;N1ICD* hearts (**B**) and throughout the myocardium of *cTnT-Cre;N1ICD* hearts (**C**). (**D**–**F**) *Bmp2* expression in WT AVC is markedly reduced in transgenic hearts. (**G**–**I**) *Tgfb2*. Expression in WT AVC is reduced in transgenic hearts. (**J**–**L**) *Anf* is restricted to WT atrium and ventricle myocardium, and is extended to AVC myocardium in transgenic hearts. (**M**–**O**) *Snail1* is expressed in WT AVC endocardium and mesenchyme (**M**) and extends throughout the myocardium and endocardium of *Nkx2.5-Cre;N1ICD* hearts (**N**) and throughout the myocardium of *cTnT-Cre;N1ICD* hearts (**O**). Scale bar: 30 μm. (**P** and **Q**) RT-PCR of E9.5 WT and *Nkx2.5-Cre;N1ICD* hearts (**P**) and *cTnT-Cre;N1ICD* hearts (**Q**).

cells with *Snail1* shRNAS. Two *Snail1* shRNAs reduced the 2D TI of *Tie2-Cre;N1ICD* ventricular explants effectively (Figure 2, M–O). RT-PCR confirmed reduced *Snail1* expression, though the reduction was greater for *Snail2* (Figure 2P), consistent with the reported requirement of Snail1 for *Snail2* expression (39). *Tgfb2* expression was also reduced by *Snail1* shRNAs (Figure 2P). This is consistent with the dose-dependent activation by Snail1 of a TGF-β2 reporter (data not shown), suggesting a functional link between Snail1 and Tgf-β2.

Ectopic endocardial N1ICD expression was examined in a stage-dependent manner using the tamoxifen-inducible line *Cdh5(PAC)-Cre^{ERT2}* (40). Recombination was induced from E9.5 to E10.5 and at E11.5, *Cdh5(PAC)-Cre^{ERT2};N1ICD* embryos showed hemorrhage in the heart and trunk region (Supplemental Figure 7, A and B) and increased *N1ICD* and *Snail1* cardiac expression (Supplemental Figure 7C). Importantly, ENCs in ventricular trabeculae showed a fibroblastic, star-like morphology, contrasting with the flat ENCs in WT trabeculae (Supplemental Figure 7, D–I). *Cdh5(PAC)-Cre^{ERT2};N1ICD* ENCs transformed and migrated in ventricular explant assays (Supplemental Figure 7, J–L) but like *Tie2-Cre;N1ICD* ENCs were not invasive.

BMP2 confers invasivity on ventricular ENCs. Functional studies have shown that Bmp2 is a critical inducer of AVC EMT upstream of Tgf-β2 (9, 10). *Bmp2* expression was unaffected in *Tie2-Cre;N1ICD* embryos (Supplemental Figure 2, E, F, and K), suggesting that Notch acts either downstream or independently of Bmp2 during cardiac EMT. BMP2 treatment of WT and *Tie2-Cre;N1ICD* ventricular explants produced invasive mesenchymal cells, significantly increasing 2D and 3D TI in WT explants and 3D TI in transgenic explants (Figure 3, A, B, D, and E, and Supplemental Video 3). Thus, BMP2 confers invasive ability to transformed ventricular ENCs. Expression of *Snail1*, *Has2*, and *Periostin* (but not *Twist1*) was upregulated in WT ventricular cells treated with BMP2 (Figure 3F), indicating that BMP2-treated WT ventricular explants acquire full mesenchymal features.

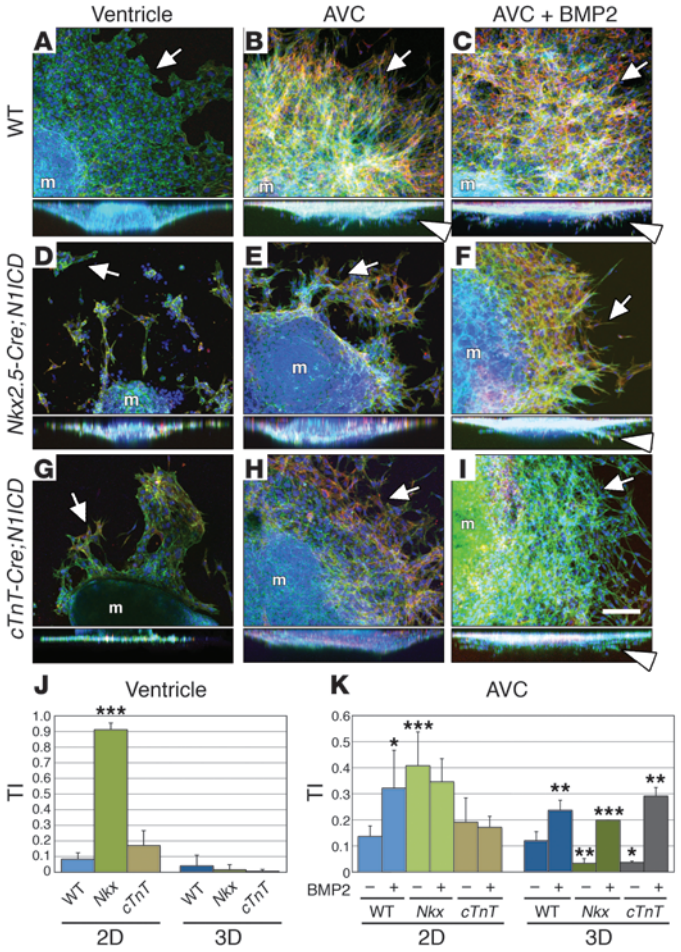

Figure 5

BMP2 treatment rescues EMT in Notch1-expressing myocardium. Heart explants triple stained as in Figure 2. (**A**–**I**) Details of explants. Full lateral views are shown below. (**A**) WT ventricular explants show an endocardial monolayer. (**B** and **C**) WT AVC explants ± BMP2 undergo EMT. (**D**) In *Nkx2.5-Cre;N1ICD* ventricular explants, ENCs migrate across the collagen surface, but are not invasive. (**E**) *Nkx2.5-Cre;N1ICD* AVC explants produce migratory mesenchymal cells that show reduced invasion, which is rescued by BMP2 (**F**). (**G**) In *cTnT-Cre;N1ICD* ventricular explants, most ENCs grow as a monolayer and are noninvasive. (**H**) Mesenchymal cells in *cTnT-Cre;N1ICD* AVC explants migrate but show reduced invasion, which is rescued by BMP2 (**I**). Arrows, ENCs; arrowheads, invasive mesenchymal cells. (**J**) TI analysis of ventricular explants. Most ENCs in *Nkx2.5-Cre;N1ICD* explants (*Nkx*) migrate over the gel surface ($P = 2.2 \times 10^{-7}$ for 2D TI versus WT explants), whereas few cells in *cTnT-Cre;N1ICD* explants (abbreviated *cTnT*) migrate in 2D. 3D TI is very low for both genotypes. (**K**) TI analysis of AVC explants. BMP2 treatment of WT explants significantly increases 2D and 3D TI ($P = 3.7 \times 10^{-2}$ and 6.1×10^{-3}). *Nkx2.5-Cre;N1ICD* explants (*Nkx*) show increased 2D TI ($P = 3.5 \times 10^{-4}$) but a markedly reduced 3D TI compared with WT ($P = 5.7 \times 10^{-3}$). BMP2 treatment increases *Nkx2.5-Cre;N1ICD* 3D TI ($P = 6.7 \times 10^{-4}$) and slightly reduced 2D TI. BMP2 treatment sharply increases the 3D TI of *cTnT-Cre;N1ICD* explants (*cTnT*; $P = 1.9 \times 10^{-3}$). m, myocardium. Scale bar: 50 μm. Results are expressed as mean + SD. $^{*}P < 0.005$; $^{**}P < 0.01$; $^{***}P < 0.001$.

Anti–TGF-β2 antibody inhibited the effect of BMP2 on WT explants (Figure 3, C and D), indicating that, as in AVC EMT, TGF-β2 acts downstream of Bmp2 during ventricular EMT. Although *Bmp6* was ectopically expressed in *Tie2-Cre;N1ICD* ventricular endocardium (Supplemental Table 1 and Supplemental Figure 4, E, F, and I), BMP6 did not induce EMT in WT ventricular explants (not shown).

To examine the requirement for Notch in BMP2-induced ventricular EMT, we cultured WT ventricular explants with BMP2 plus the γ-secretase inhibitor N-[N-(3,5-difluorophenacetyl)-l-alanyl]-S-phenylglycine t-butyl ester (DAPT) (41). DAPT reduced invasion after 72 hours, increasing 2D TI while reducing 3D TI (Figure 3, G–I). Thus, inhibition of Notch in BMP2-treated WT ventricular explants led to accumulation of scattered cells that did not invade. BMP2-induced invasion and 3D TI were similarly reduced in WT ventricular explants transduced with *Snail1-shRNA* (Figure 3, J–L). Thus, Tgf-β2, Notch, and Snail1 participate in the molecular mechanism underlying BMP2-induced invasive EMT in ventricular explants.

Myocardial-specific Notch1 activation leads to Bmp2 and Tgfb2 repression and ectopic Snail1 expression. Studies in chick and mouse have shown that Hey transcription factors repress *Bmp2* expression in chamber myocardium, restricting it to AVC and OFT territory (42, 43). To determine whether myocardially expressed N1ICD impaired endocardial EMT via Hey-mediated *Bmp2* repression, we used the *Nkx2.5-Cre* driver line, which is active in both endocardium and myocardium from E7.5 (44). Supplemental Figure 8A shows Cre reporter activity in these tissues at E9.5. N1ICD-GFP was expressed throughout the heart of *Nkx2.5-Cre;N1ICD* embryos (Supplemental Figure 8B). At E9.5, *Nkx2.5-Cre;N1ICD* embryos showed pericardial distension and heart dilation, with poorly defined boundaries between chamber and nonchamber tissue, an AVC region devoid of transformed cells, and a thin ventricular myocardium with underdeveloped trabeculae (Supplemental Figure 8, C–G). *Hey1* was expressed throughout the myocardium and endocardium, including the AVC (Figure 4, A and B). The expanded *Hey1* domain was reflected in increased transcription by RT-PCR (Figure 4P). Myocardial *Hey2* and *Heyl* expression was unaltered (not shown), but was increased overall (Figure 4P and data not shown) due to stronger endocardial expression.

The ectopic *Hey1* expression was accompanied by reduced *Bmp2* in *Nkx2.5-Cre;N1ICD* AVC myocardium (Figure 4, D, E, and P). *Tgfb2* transcription in AVC myocardium (Figure 4G) was strongly reduced in transgenic embryos (Figure 4, H and P). Expression of the myocardial chamber marker *Anf* was expanded to the AVC (Figure 4, J, K, and P), suggesting that AVC identity was lost in myocardial cells. *Snail1* was exclusively expressed in AVC and OFT endocardium and mesenchyme of WT embryos (Figure 4M), while Snail1 transcript and protein were ectopically expressed throughout the endocardium and myocardium of *Nkx2.5-Cre;N1ICD* embryos (Figure 4N and data not shown).

To substantiate these findings, Notch1 was activated exclusively in the myocardium by breeding into the *cTnT-Cre* line, which is active in every heart segment from E7.5 onwards (45). Supplemental Figure 8H shows myocardial Cre reporter activity at E9.5.

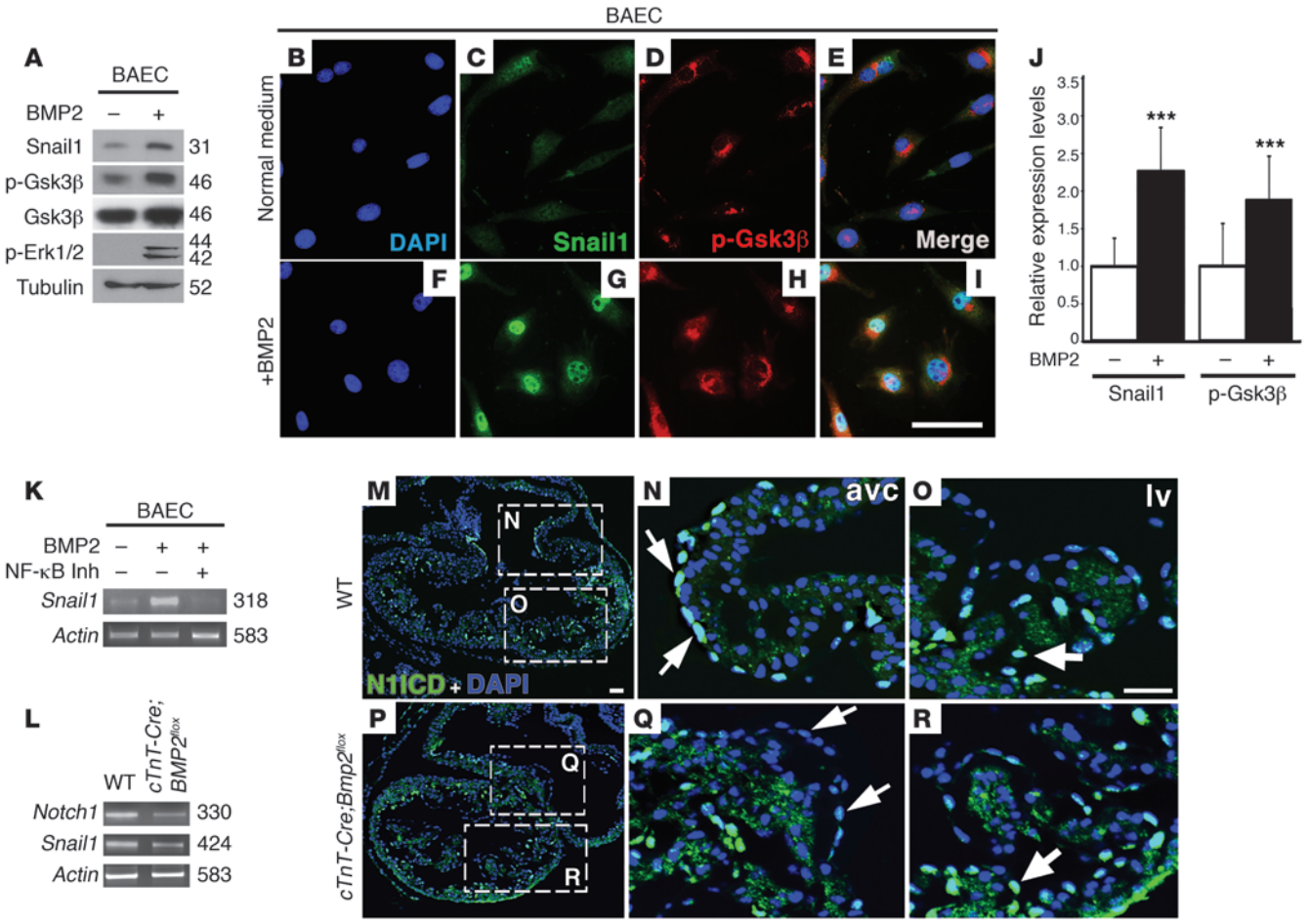

Figure 6

BMP2 inhibits Gsk3β, leading to *Snail1* expression and nuclear stabilization. Deletion of myocardial *Bmp2* reduces Notch1 signaling in AVC. (**A**) Immunoblot of BAECs cultured ± BMP2. Weak Snail1 expression is detected in the absence of BMP2. BMP2 induces increased Snail1 levels and increases phosphorylation of Gsk3β and Erk1/2, suggesting Gsk3β inhibition. (**B**–**I**) Immunostaining of BAECs cultured ± BMP2. (**B** and **F**) DAPI-counterstained nuclei. (**C** and **G**) Snail1 expression; nuclear staining in BMP2-treated cells is stronger and more punctate. (**D** and **H**) p-Gsk3β; predominant perinuclear p-Gsk3β staining is stronger after BMP2 treatment. (**E** and **I**) Merged showing DAPI, Snail1, and p-Gsk3β staining. (**J**) Quantification of Snail1 and p-Gsk3β protein. Expression is increased upon BMP2 treatment. (**K**) RT-PCR analysis of *Snail1* expression in BAECs cultured ± BMP2 and ± NF-κB inhibitor. *Snail1* expression is reduced in the presence of BMP2 and NF-κB inhibitor. (**L**) RT-PCR of E10.5 WT and *cTnT-Cre;Bmp2*^{flox} hearts. *Notch1* and *Snail1* expression is reduced in mutant hearts. (**M**–**R**) N1ICD immunostaining (green). Nuclei are DAPI counterstained (blue). (**M**–**O**) E10 WT heart. (**P**–**R**) *cTnT-Cre;Bmp2*^{flox} heart. (**M** and **P**) General views. (**N** and **Q**) AVC detail. Arrows mark N1ICD-positive nuclei in WT AVC endocardium (**N**) and weakly positive nuclei in the corresponding region of the mutant (**Q**). (**O** and **R**) Detail of LV. Arrows mark N1ICD-positive nuclei in endocardium at the base of trabeculae in WT (**O**) and mutant embryos (**R**). Scale bars: 20 μm. Results are expressed as mean + SD. ***$P < 0.001$.

cTnT-Cre;N1ICD embryos expressed N1ICD-GFP throughout the myocardium (Supplemental Figure 8I). E10.5 transgenic embryos were smaller than WT and showed pericardial distension, poorly defined cardiac regions, and a lack of mesenchymal cells in the AVC (Supplemental Figure 8, J–M). Trabeculae were apparent (Supplemental Figure 8, L and N) but slightly delayed compared with WT embryos (Supplemental Figure 1, B and F). *Hey1* was expressed throughout the myocardium of *cTnT-Cre;N1ICD* embryos, including the AVC (Figure 4C and data not shown), and was increased (Figure 4Q). *Bmp2* and *Tgfb2* expression were reduced (Figure 4, F, I, and Q), and as in *Nkx2.5-Cre;N1ICD* embryos, *Anf* expression was extended to AVC myocardium (Figure 4, L and Q), suggesting loss of AVC identity. Likewise, *Snail1* was abnormally expressed in the myocardium (Figure 4O) and increased (Figure 4Q).

The aberrant *Hey1* and *Bmp2* expression in the myocardium of *Nkx2.5-Cre;N1ICD* and *cTnT-Cre;N1ICD* embryos supports the idea that N1ICD-driven ectopic *Hey1* expression represses *Bmp2* in AVC myocardium. *Hey* and *Bmp2* expression were examined in Notch loss of function (LOF) (Supplemental Figure 9). The expression of *Hey1* and *Hey2* was detected in chamber myocardium (Supplemental Figure 9, A and C). *Hey1* was also found in atrial endocardium (Supplemental Figure 9A), *Hey2* throughout the endocardium (Supplemental Figure 9C), and *Heyl* in AVC endocardium (Supplemental Figure 9E). In *RBPJk* mutants, myocardial *Hey1* and *Hey2* expression were unaffected (Supplemental Figure 9, B and D), whereas endocardial *Hey* gene expression was reduced (Supplemental Figure 9, B, D, F, and I). In *RBPJk* mutants (Supplemental Figure 9, G and H), *Bmp2* expression was not

affected in the myocardium but was upregulated in the endocardium (Supplemental Figure 9, H and I). These data suggest that *Hey2* acts downstream of Notch in repressing *Bmp2* expression in the endocardium.

Ectopic myocardial Notch1 activity impairs EMT in a Bmp2-dependent fashion. To study the effect of deregulated *Bmp2* and *Snail1* expression on EMT, we performed cardiac explant experiments with E9.5 *Nkx2.5-Cre;N1ICD* and *cTnT-Cre;N1ICD* embryos. As expected, WT ventricular endocardium grew as a monolayer (Figure 5A) with a few scattered ENCs at the explant edge and almost no invasion (Figure 5J). WT AVC explants showed ENC outgrowth and several invading mesenchymal cells (Figure 5B), with 2D and 3D TI between 0.1 and 0.15 (Figure 5K). Addition of BMP2 significantly increased surface migration and invasion (Figure 5C and Supplemental Video 3), reflected in 2D and 3D TI values of greater than 0.3 and greater than 0.2 (Figure 5K).

Ventricular explants of *Nkx2.5-Cre;N1ICD* embryos generated scattered, noninvasive ENCs (Figure 5D) with a 2D TI (0.9) significantly higher than that of WT explants (Figure 5J). *Nkx2.5-Cre;N1ICD* AVC explants (Figure 5E and Supplemental Video 4) showed relatively high surface migration (2D TI = 0.4; Figure 5K) but severely reduced invasion (3D TI < 0.1; Figure 5K). Addition of BMP2 restored the WT phenotype (3D TI = 0.2; Figure 5, F and K, and Supplemental Video 4).

cTnT-Cre;N1ICD ventricular explants behaved similarly to WT ventricular explants, with no endocardial transformation (Figure 5, G and J), consistent with the lack of ectopically activated endocardial Notch1 in this model. *cTnT-Cre;N1ICD* AVC explants (Figure 5H) transformed very poorly (3D TI < 0.1; Figure 5K), but addition of BMP2 restored invasiveness (3D TI = 0.3; Figure 5, I and K).

These data indicate that Notch1 activation in endocardium endows chamber ENCs with transforming ability. Notch1 activation in myocardium leads to *Bmp2* and *Tgfb2* downregulation by ectopic *Hey1* expression.

Bmp2 promotes Snail1 expression and stability, and its inactivation impairs Notch1 signaling in AVC. During EMT, SNAIL1 is regulated by 2 sequential GSK3β-mediated phosphorylation events. The first SNAIL1 phosphorylation event induces nuclear export; the second, proteasomal degradation (46). In endothelial cells, BMP2 induces ERK1/2 phosphorylation (activation), which itself phosphorylates (inactivates) GSK3β (47). We tested the putative link among Bmp2 signaling, Gsk3β inhibition, and Snail1 stabilization in ENCs. Immunoblotting of bovine aortic endothelial cells (BAECs) incubated with the proteasome inhibitor MG132 (46) detected a 31-kDa Snail1 band, while the levels of p-Gsk3β and p-Erk1/2 were low (Figure 6A). Addition of BMP2 markedly increased Snail1 expression as well as the levels of p-Gsk3β and p-Erk1/2, while the total amount of Gsk3β was unaffected (Figure 6A). Immunofluorescence of unstimulated BAECs detected weak nuclear Snail1 expression (Figure 6, B and C) and faint, predominantly perinuclear staining of p-Gsk3β (Figure 6, D and E). In BMP2-treated BAECs, Snail1 nuclear staining was increased (120% increase) and perinuclear p-Gsk3β staining was also stronger (80%; Figure 6, G–J).

In epithelial cells, Gsk3β has also been shown to regulate Snail1 at the transcriptional level, together with Gsk3α, via NF-κB inhibition (48). We tested to determine whether this mechanism contributes to the effect of BMP2 in BAECs. Figure 6K shows that adding BMP2 to BAECs markedly increased *Snail1* mRNA while BMP2 plus an NF-κB inhibitor markedly reduced it. We tested the effect of NF-κB inhibition on the BMP2-driven EMT of ventricular explants. WT ventricular explants cultured with BMP2 underwent invasive EMT (Supplemental Figure 10, A and C), which was notably reduced when an NF-κB inhibitor was added to the culture medium (Supplemental Figure 10, B and C). This effect was also reflected by the marked reduction of *Snail1* mRNA upon addition of the NF-κB inhibitor (Supplemental Figure 10D). Together these observations suggest that BMP2 treatment of endothelial cells augments *Snail1* mRNA in an NF-κB–dependent manner and stabilizes Snail1 protein by Gsk3β phosphorylation/ inactivation.

Our data show that Bmp2 and Notch1 cooperate to induce invasive EMT in ventricular explants. This process is Notch dependent, and the noninvasive phenotype of AVC explants ectopically expressing Notch1 in the myocardium is rescued by exogenous BMP2. To explore the Bmp2-Notch1 relationship in vivo, we crossed a conditional *Bmp2* mutant (49) with the myocardial-specific *cTnT-Cre* driver line. E10.5 *cTnT-Cre;Bmp2*^{flox} embryos lacked defined AVC and EC tissue (Supplemental Figure 11, A–F), similar to the phenotype obtained with the *Nkx2.5-Cre* driver (10, 11). Cardiac expression of *Notch1* (and *Snail1*) was markedly reduced (Figure 6L), which, given the exclusive endocardial *Notch1* expression at this stage, suggests that myocardial *Bmp2* deletion impairs endocardial *Notch1* expression. In E10 WT embryos, N1ICD is localized in most ENCs in the AVC and to ENCs at the base of trabeculae in the ventricles (Figure 6, M–O, and ref. 14). In *cTnT-Cre;Bmp2*^{flox} mutants, N1ICD staining was strongly reduced in AVC endocardium (Figure 6, P and Q) but ventricular staining was unaffected (Figure 6, P and R). These data suggest that *Bmp2* deletion in the myocardium specifically impairs Notch1 expression and activity in AVC endocardium.

Discussion

We previously showed that Notch is a key signal during CVF that via *Snail1* activation, promotes the EMT of ENCs to form the valve primordium (12). Notch/RBPJK directly regulate *Snail1* transcription (12, 50), and Notch inactivation leads to a downregulation of *Snail1* expression in AVC endocardium (12). This earlier report did not, however, provide information about the role of Notch targets in EMT and neither did it define the domain-specific (chamber vs. nonchamber) and tissue-specific (endocardium vs. myocardium) patterning of Notch function or determine the extent of Notch interaction with myocardial signals that trigger EMT (e.g., Tgf-β2 and Bmp2). The main goal of the present report was to shed light on the integration of EMT-driving signals and the establishment of valve developmental domains in the embryonic heart.

Transgenic mice constitutively expressing N1ICD throughout the endocardium, myocardium, or both have allowed us to establish Notch as a key endocardial signal that acts in concert with myocardial Bmp2 to promote a valve-forming field in the developing heart. We propose that Snail1 is a critical point of convergence between Notch1 and Bmp2 signaling based on the following experimental evidence: (a) ectopic N1ICD expression in either endocardium or myocardium leads to *Snail1* upregulation in these tissues; (b) the noninvasive EMT of *Tie2-CRE;N1ICD* ENCs in ventricular explants is mediated by Snail1, and the complete EMT driven by BMP2 is also Snail1-dependent; (c) targeted *Bmp2* inactivation in the myocardium leads to reduced *Snail1* expression in AVC endocardium (ref. 10 and this report); and (d) BMP2 stimulation increases Snail1 expression in BAECs.

An important issue raised by these findings is how these signals are restricted to specific tissues and their activities coordinated.

Two reports have examined the effect of ectopic Notch1 activation on cardiovascular development. In the first study, Notch1 was activated in cardiogenic mesoderm using the *Mesp1-Cre* driver line, demonstrating that transgenic mice show defective AVC myocardial differentiation and ventricular maturation (19). Similarly to WT embryos, the AVC of transgenic embryos contained mesenchymal cells, but also showed ectopic myocardial masses of uncertain origin. Since N1ICD activation occurred in both endocardium and myocardium, these authors did not study the specific effect of Notch1 activation in either of these layers (19). The second study used the *Tie2-Cre* driver line to express N1ICD in the endocardium and vascular endothelium (51). These authors reported defective trabeculation, thinner myocardium, and delayed endocardial cushion formation, but the cellular and molecular bases of these defects were not examined.

Our results provide the first demonstration of the expansion of the characteristic AVC-restricted transcription of Notch target genes (*Hey1*, *Heyl*, *Dll4*, *c-myc*, and *Nrarp*) to the ventricular endocardium after N1ICD overexpression in this tissue (*Tie2-Cre;N1ICD*). In light of earlier observations that *Hey1* and *Dll4* are downregulated in *RBPJk* and *Notch1* mutants (12), we suggest that Notch target gene expression is regulated by a positive feedback loop and that Notch signals in the endocardium by lateral induction, with AVC ENCs behaving as a developmental field. We find a set of genes involved in EMT, cell migration, metastasis, and invasion to be upregulated and ectopically expressed in the ventricular endocardium of *Tie2-Cre;N1ICD* embryos (Supplemental Table 1). These data indicate that WT Notch1 activity in AVC ENCs promotes EMT by driving, in a cell-autonomous manner, a mesenchyme gene program that can be experimentally extended to the ventricles by endocardial *NICD* overexpression. This notion is consistent with the downregulation of the endocardial chamber marker *Irx5*, suggesting that ventricular ENCs of *Tie2-Cre;N1ICD* embryos have lost their chamber identity.

AVC explants of *Tie2-Cre;N1ICD* embryos undergo EMT, with ENCs invading the collagen matrix (3D EMT) and showing increased migratory capacity on the gel surface (2D EMT) with respect to WT AVC. In contrast to the characteristic EMT-refractory ventricular endocardium of WT mice, ENCs of *Tie2-Cre;N1ICD* ventricular explants (or those from *Cdh5[PAC]-Cre^{ERT2};N1ICD* mice) generate mesenchymal cells expressing *Snail1*, *Snail2*, and *Tgfb2* that lose contact and scatter over the gel surface, but are unable to invade the gel matrix. Addition of TGF-β2 can mimic this effect in WT ventricular endocardium, whereas lentiviral- or antibody-mediated inhibition of *Snail1* and Tgf-β2 inhibits transformation of *Tie2-Cre;N1ICD* explants, indicating that these molecules lie downstream of Notch in EMT. Thus, Notch alone is able to promote noninvasive EMT in a Snail1 and Tgf-β2–dependent manner, but cannot trigger a fully invasive EMT. WT ventricular ENCs become fully invasive after BMP2 addition and inhibition of Notch, Tgf-β2, or *Snail1* severely attenuates BMP2-induced invasion, indicating that Notch and Bmp2 are critical signals acting in concert during EMT.

Constitutive Notch1 activation in the myocardium (*Nkx2.5-Cre;N1ICD* or *cTnT-Cre;N1ICD*) caused cardiac dysmorphogenesis. The expansion of myocardial chamber markers *Anf* and *Chisel* to the AVC and the *Hey1* upregulation and concomitant *Bmp2* downregulation in AVC myocardium suggested that myocardial cells have lost their AVC identity. Thus, ectopic myocardial Notch activity — via the activation of *Hey1* — prevents *Bmp2* expression in chamber myocardium, supporting the idea that Hey proteins regulate *Bmp2* expression and thus AVC patterning (42, 43). Loss of *Bmp2* expression is consistent with the poor ENC invasion observed in AVC explants from *cTnT-Cre;N1ICD* embryos. Remarkably, *Snail1* expression is upregulated in both the endocardium and myocardium of *Nkx2.5-Cre;N1ICD* embryos, whereas *Bmp2* is downregulated in the AVC (presumably via ectopic Hey1 activity), in agreement with the very poor transforming ability of AVC explants from these embryos. The rescue of invasiveness by BMP2 indicates that this molecule is critical for the acquisition of invasiveness by ENCs and that Notch promotes the transformed mesenchymal phenotype in AVC or OFT endocardium. Thus, Notch is likely to cooperate with Bmp2 to promote full deployment of invasive properties by transformed ENCs.

What is the role of Notch, Bmp2, and Hey in cardiac patterning? Supplemental Figure 12 summarizes the data from studies of Notch (this report and ref. 19) and *Hey1* and *Hey2* (42, 43) gain of function (GOF) and LOF, in terms of their effect on the *Bmp2* expression domain and cardiac patterning. In the myocardium, *Bmp2* expression is confined to the AVC by Hey1 and Hey2, which are expressed in the chambers (ref. 42 and 43, and Supplemental Figure 12A). In the endocardium, Notch1-dependent *Hey1*, *Hey2*, and *Heyl* are differentially expressed in the AVC and chambers and repress *Bmp2* (Supplemental Figure 9 and Supplemental Figure 12A). Ectopic *N1ICD* expression in endocardium expands AVC patterning to ventricular endocardium but does not affect *Hey1*, *Hey2*, or *Bmp2* myocardial expression or patterning (Supplemental Figure 12B). Ectopic *N1ICD* expression in the myocardium leads to expansion of *Hey1* and loss of *Bmp2* expression, and chamber markers expand to the AVC (Figure 4, K and L, and Supplemental Figure 12C). In both N1ICD GOF models, *Bmp2* is repressed in the endocardium, similarly to the WT situation. Systemic abrogation of Notch signaling leads to downregulation of *Hey* genes and ectopic endocardial *Bmp2* expression, indicating that Notch represses *Bmp2* in the endocardium via Hey proteins (Supplemental Figure 9 and Supplemental Figure 12D) and suggesting that Notch might normally prevent ENCs from acquiring primitive cardiomyocyte features, such as those of the AVC. Notch inactivation impairs endocardial patterning of the AVC and chambers (refs. 12 and 52, and Supplemental Figure 12D), but does not affect myocardial patterning or the myocardial expression domains of *Hey1*, *Hey2*, or *Bmp2* (Supplemental Figure 9 and Supplemental Figure 12D).

Our findings also shed light on how Notch1 and Bmp2 signals are integrated to promote EMT. Our data establish that Bmp2 triggers full EMT in WT and *Tie2-Cre;N1ICD* ventricular explants and that cell invasion in WT explants can be markedly reduced by inhibiting Tgf-β2, Notch, or Snail1. This supports the idea that these molecules are required for Bmp2-driven invasive EMT and indicate that Bmp2 and Notch1 signaling converge during AVC (and OFT) differentiation and the establishment of EMT competence in ENCs. At least 2 lines of evidence suggest that Bmp2 acts upstream of endocardial Notch activity during cardiac EMT: (a) impaired Notch1-Snail1–dependent signaling in AVC endocardium of *Bmp2* myocardial mutants (*cTnT-Cre; BMP2^{flox}*) indicates that Bmp2 is required for Notch activity in AVC territory; (b) *Notch* deficiency, while blocking transformation in vivo and in vitro by loss of *Snail1* expression (12), does not affect *Bmp2* expression in AVC myocardium (Supplemental Figure 9H). Moreover, ectopic Notch activity in endocardium upregu-

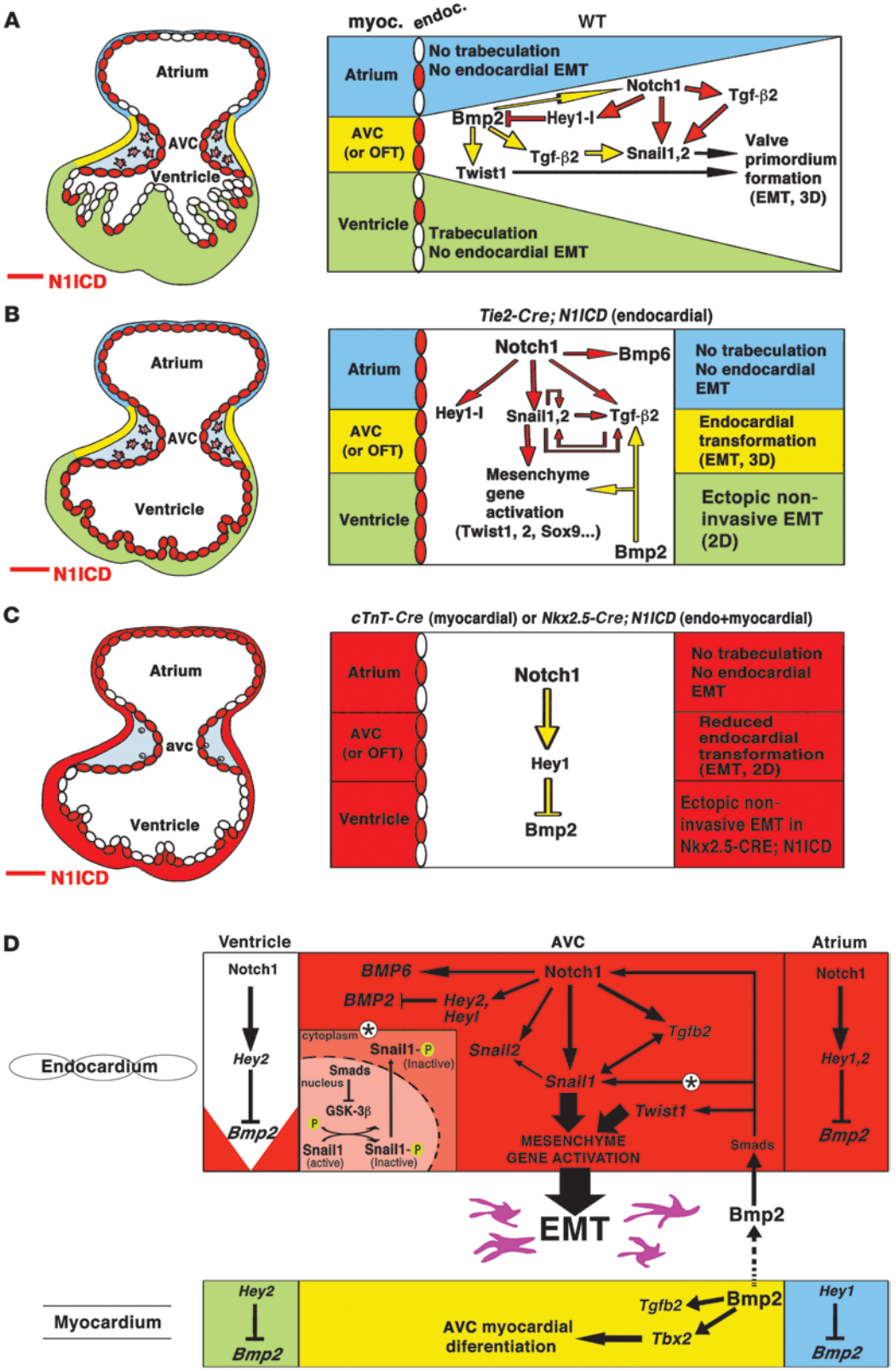
A
Atrium
AVC
Ventricle
N1ICD
myoc.
endoc.
WT
Atrium
No trabeculation
No endocardial EMT
Notch1
Tgf-β2
Bmp2
Hey1-I
AVC
(or OFT)
Tgf-β2
Snail1,2
Valve
primordium
formation
(EMT, 3D)
Twist1
Ventricle
Trabeculation
No endocardial EMT
B
Atrium
AVC
Ventricle
N1ICD
Tie2-Cre; N1ICD (endocardial)
Atrium
Notch1
Bmp6
No trabeculation
No endocardial
EMT
Hey1-I
Snail1,2
Tgf-β2
AVC
(or OFT)
Endocardial
transformation
(EMT, 3D)
Mesenchyme
gene
activation
(Twist1, 2, Sox9...)
Ventricle
Ectopic non-
invasive EMT
(2D)
Bmp2
C
Atrium
avc
Ventricle
N1ICD
cTnT-Cre (myocardial) or Nkx2.5-Cre; N1ICD (endo+myocardial)
Atrium
Notch1
No trabeculation
No endocardial
EMT
AVC
(or OFT)
Hey1
Reduced
endocardial
transformation
(EMT, 2D)
Ventricle
Bmp2
Ectopic non-
invasive EMT in
Nkx2.5-CRE; N1ICD
D
Ventricle
AVC
Atrium
Notch1
BMP6
Notch1
Notch1
BMP2
Hey2,
Hey1
Tgfb2
cytoplasm
Snail1- P
(Inactive)
Hey2
Snail2
Endocardium
Smads
nucleus
Snail1
Hey1,2
GSK-3β
Twist1
Bmp2
Snail1
(active)
Snail1- P
(Inactive)
MESENCHYME
GENE ACTIVATION
Smads
Bmp2
EMT
Bmp2
Hey2
Tgfb2
Bmp2
Hey1
Myocardium
AVC myocardial
diferentiation
Tbx2
Bmp2
Bmp2

Figure 7
A model for concerted Notch1 and Bmp2 activities in CVF. Left, schematic representations of the E9.5 heart. Right, schematics showing the different cardiac regions and developmental processes occurring within them. Green, ventricular myocardium; yellow, AVC myocardium; blue, atrial myocardium. ENCs expressing N1ICD are labeled red. Pink, invasive mesenchyme cells. Yellow arrows, myocardial signals; red arrows, endocardial signals. (**A**) WT embryo. AVC myocardial Bmp2 is required for *Tgfb2*, *Notch1*, *Snail1*, *Snail2*, and *Twist1* expression. Endocardial Notch1 is required for *Tgfb2* expression, activates *Snail1* and *Snail2*, and represses *Bmp2* in endocardium via Hey proteins. Bmp2 and Notch1 signals converge in AVC endocardium to promote complete EMT. (**B**) *Tie2-Cre;N1ICD* embryo. Ectopic N1ICD expression in endocardium (left) activates mesenchymal genes, promotes noninvasive EMT in ventricles but not in atria, and leads to loss of chamber identity. (**C**) *cTnT-Cre;N1ICD* and *Nkx2.5-Cre;N1ICD* embryos. Ectopic N1ICD expression in myocardium leads to ectopic *Hey1* expression and *Bmp2* repression. Myocardial AVC identity is lost, and EMT is severely affected. (**D**) Molecular pathways downstream of Notch during cardiac EMT. LOF and GOF data (this report and refs. 19, 42, and 43) indicate that Notch represses *Bmp2* via *Hey* target activation. Endocardial Notch1 activates a mesenchyme gene program. The double-headed arrow linking *Tgfb2* and *Snail1* indicates the interdependence of both genes. Myocardial Bmp2 converges with endocardial Notch1 signaling to promote mesenchyme gene activation and EMT in the AVC. Convergence of Notch1 and Bmp2 is reflected in Notch activation of *Snail1* expression and Bmp2-mediated Snail1 nuclear stabilization, via Gsk3β inhibition (*).

lates and expands Snail1-dependent expression of *Twist2*, but not that of Bmp2-dependent *Twist1* (10), suggesting that Bmp2 and Notch1 elicit overlapping but different mesenchyme gene expression programs in the AVC endocardium.

The concerted activities of Notch1 and Bmp2 in valve formation are reflected in the activation of *Snail1* expression in chamber endocardium in response to ectopic Notch1 activity and in the reduced *Snail1* expression after myocardial *Bmp2* deletion. Moreover, inhibition of Gsk3β in BMP2-stimulated BAECs suggests that whereas Notch1 promotes *Snail1* expression, Bmp2 stimulates both *Snail1* expression and protein stabilization by inhibiting Gsk3β activity. The interplay between Notch and Bmp2 during the acquisition of the invasive phenotype by AVC ENCs involves Notch1- and Bmp2-induced *Snail1* expression and Bmp2-mediated Snail1 nuclear accumulation, leading to sustained expression of mesenchymal genes. This provides what we believe is a novel mechanism for the integration of Notch1 and Bmp2 activity in EMT. Our results, summarized in Figure 7, emphasize the importance of endocardium-myocardium interplay during CVF and suggest that endocardial Notch1 converges with myocardial Bmp2 to promote and regulate the extent of EMT in prospective valve territory in both the AVC and OFT.

The results presented in this study open new avenues of research into the origin of cardiac valves and septal defects, which are the most common types of cardiac congenital abnormality and a major cause of adult morbidity and mortality (1, 53). Moreover, alterations of any component of the embryonic Notch1-Bmp2-Snail1 axis described here might be relevant in calcific aortic valve stenosis (4) or atherosclerosis (54), as these diseases share features such as EMT, fibrosis, and calcification. This analysis will be instrumental in the dissection of the cellular and molecular components of cardiac valve disease, the prevalent condition among congenital heart anomalies.

Methods

Mouse strains. Mouse strains were *R26N1ICD* (20), *Bmp2^{flox}* (49), *RBPJk* (55), *Tie2-Cre* (21), *Nkx2.5-Cre* (44), *cTnT-Cre* (45), and *Cdh5(PAC)-Cre^{ERT2}* (40). For simplicity, we use *Tie2-Cre;N1ICD* to refer to *Tie2-Cre/+;R26N1ICD/+* mice, *Nkx2.5-Cre;N1ICD* for *Nkx2.5-Cre/+;R26N1ICD/+* mice, *cTnT-Cre;N1ICD* for *cTnT-Cre/+;R26N1ICD/+* mice, *Cdh5(PAC)-Cre^{ERT2};N1ICD* for *Cdh5(PAC)-Cre^{ERT2}/+;R26N1ICD/+* mice and *cTnT-Cre;Bmp2^{flox}* for *cTnT-Cre/+;Bmp2$^{flox/flox}$* mice. *R26N1ICD* mice were provided by D.A. Melton (Harvard University, Cambridge, Massachusetts, USA), and *Nkx2.5-Cre* mice were provided by R.P. Harvey (Victor Chang Cardiac Research Institute, Darlinghurst, Australia). *cTnT-Cre* driver lines were provided by S. Evans (University of California San Diego, La Jolla, California, USA). *Bmp2* conditional lines were provided by V. Rosen (Harvard University School of Dental Medicine, Boston, Massachusetts, USA). Details are provided in Supplemental Data and Supplemental Table 2.

All experimental procedures and protocols were approved by the Ethics Committee and Animal Welfare Committee of the CNIC and conformed to European Union guidelines for the care and use of laboratory animals.

AVC and LV explants. A solution (1.5 mg/ml) of rat-tail collagen type I (BD Biosciences) was dispensed into 4-well microculture dishes and allowed to solidify inside a 37°C, 5% CO_2 incubator. Collagen gels were washed several times with DMEM containing 8% FBS, 0.1% insulin-transferrin-seleniun (ITS, GIBCO; Invitrogen), and antibiotics, and drained. AVCs were harvested in sterile PBS from E9.5 or E11.5 embryos. LV were carefully dissected, avoiding contamination from AVC tissue. Explants were placed with the endocardium face down and allowed to attach (16 hours, 37°C, 5% CO_2). Medium (100 μl/well in AVC explants or 50 μl/well in LV) was added and explants cultured for up to 3 days (AVC) or 4 days (LV). Explants were fixed and stained with phalloidin-FITC (1:100; Sigma-Aldrich) to reveal the actin cytoskeleton and α-SMA-Cyan3 (1:100; Sigma-Aldrich) to detect mesenchymal cells as described (34). Explants were mounted on excavated slides in Vectashield medium containing DAPI. For explant treatments, the medium was supplemented with human TGF-β2 (30 ng/ml; Peprotech), human BMP2 (200 ng/ml; R&D Biosciences), anti-human TGF-β2 antibody (1 μg/ml; R&D Biosciences), or NF-κB SN50 inhibitor (18 μM; Calbiochem). For treatments with DAPT (γ-secretase inhibitor IX; 565770; Calbiochem), collagen gels were conditioned in explant media containing 50 μM DAPT or vehicle (ethanol). Medium was replaced every 24 hours.

Lentivirus production and Snail shRNA interference. Pseudotyped lentivectors were produced according to ref. 56. Subconfluent HEK293T cells cultured in 10-cm plates with DMEM-Glutamax (Invitrogen), 10% FBS, and antibiotics were transiently cotransfected using Lipofectamine Plus (Invitrogen) with the following plasmids: 5 μg LV-eGFP control vector or lentiviral Snail-shRNA vectors TRCN0000096620 and TRCN000009622 (mission shRNA library; Sigma-Aldrich), 5 μg packaging plasmid pCMVdR8.74, and 2 μg vesicular stomatitis virus G envelope protein plasmid pMD2G (plasmid 12259; Addgene). Supernatants were collected after 2 days and added together with polybrene (10 μg/ml) to ventricular explants on collagen gels. Snail mAb was provided by I. Virtanen (University of Helsinki, Helsinki, Finland).

Histology, lacZ staining, and in situ hybridization. See Supplemental Data.

Immunohistochemistry. See Supplemental Data.

Confocal imaging. See Supplemental Data.

Statistics. The TI of AVC and ventricular explants is the ratio of the number of scattered cells (2D migration) or the number of cells invading the collagen gel (3D migration) to the total number of cells (2D cells + 3D cells + nonmigrating ENCs) as follows: 2D TI = 2D/(2D + 3D + nonmigrating ENCs); 3D TI = 3D/(2D + 3D + nonmigrating ENCs).

Cell numbers were determined by counting DAPI-stained nuclei in the Z stack, distinguishing between 2D migrating cells, 3D migrating cells,

and nonmigrating ENCs. At least 15 explants were assayed per genotype and condition.

Results are expressed as mean + SD. An unpaired 2-tailed Student's *t* test was performed to assess differences among groups. $P < 0.05$ was considered significant.

RNA isolation and semiquantitative RT-PCR. See Supplemental Data. For primers and conditions, see Supplemental Table 3.

Microarray hybridization and scanning. See Supplemental Data.

Western blot. See Supplemental Data.

Acknowledgments

We thank D.A. Melton for the *R26N1ICD* mice; R.P. Harvey for the *Nkx2.5-Cre* mice; S. Evans for the *cTnT-Cre* driver lines; V. Rosen for the *Bmp2* conditional lines; I. Virtanen for the Snail mAb; A. García-Herreros, F.J. Díaz-Benjumea and D. MacGrogan for helpful discussions; M. Manzanares for critical reading of the manuscript; and S. Bartlett for English editing. L. Luna-Zurita is supported by a fellowship linked to grant LSHM-CT-2005-018630 (HeartRepair, European Union FP6) and the Spanish Society of Cardiology. The CNIC is supported by the Spanish Ministry of Science and Innovation and the Pro-CNIC Foundation. This work was funded by grants SAF2007-62445 (Spanish Ministry of Science and Innovation), P-2006/BIO-194 (Regional Government of Madrid), RD06/0014/0038 and RD06/0010/1013 (Spanish Ministry of Health), and LSHM-CT-2005-018630 (HeartRepair, European Union FP6) to J.L. de la Pompa.

Received for publication February 14, 2010, and accepted in revised form August 4, 2010.

Address correspondence to: José Luis de la Pompa, Laboratorio de Biología Celular y del Desarrollo, Dpto. de Biología del Desarrollo Cardiovascular, Centro Nacional de Investigaciones Cardiovasculares (CNIC), Melchor Fernández Almagro 3, E-28029 Madrid, Spain. Phone: 34.91.4531334; Fax: 34.91.4531304; E-mail: jlpompa@cnic.es.

Joaquim Grego-Bessa's present address is: Sloan-Kettering Institute, New York, New York, USA.

1. Loffredo CA. Epidemiology of cardiovascular malformations: prevalence and risk factors. *Am J Med Genet*. 2000;97(4):319–325.
2. Siu SC, Silversides CK. Bicuspid aortic valve disease. *J Am Coll Cardiol*. 2010;55(25):2789–2800.
3. Joziasse IC, et al. Genes in congenital heart disease: atrioventricular valve formation. *Basic Res Cardiol*. 2008;103(3):216–227.
4. Garg V, et al. Mutations in NOTCH1 cause aortic valve disease. *Nature*. 2005;437(7056):270–274.
5. Person AD, Klewer SE, Runyan RB. Cell biology of cardiac cushion development. *Int Rev Cytol*. 2005;243:287–335.
6. Markwald RR, Fitzharris TP, Manasek FJ. Structural development of endocardial cushions. *Am J Anat*. 1977;148(1):85–119.
7. Boyer AS, Ayerinskas II, Vincent EB, McKinney LA, Weeks DL, Runyan RB. TGFbeta2 and TGFbeta3 have separate and sequential activities during epithelial-mesenchymal cell transformation in the embryonic heart. *Dev Biol*. 1999; 208(2):530–545.
8. Camenisch TD, et al. Temporal and distinct TGFbeta ligand requirements during mouse and avian endocardial cushion morphogenesis. *Dev Biol*. 2002;248(1):170–181.
9. Sugi Y, Yamamura H, Okagawa H, Markwald RR. Bone morphogenetic protein-2 can mediate myocardial regulation of atrioventricular cushion mesenchymal cell formation in mice. *Dev Biol*. 2004;269(2):505–518.
10. Ma L, Lu MF, Schwartz RJ, Martin JF. Bmp2 is essential for cardiac cushion epithelial-mesenchymal transition and myocardial patterning. *Development*. 2005;132(24):5601–5611.
11. Rivera-Feliciano J, Tabin CJ. Bmp2 instructs cardiac progenitors to form the heart-valve-inducing field. *Dev Biol*. 2006;295(2):580–588.
12. Timmerman LA, et al. Notch promotes epithelial-mesenchymal transition during cardiac development and oncogenic transformation. *Genes Dev*. 2004;18(1):99–115.
13. Kopan R, Ilagan MX. The canonical Notch signaling pathway: unfolding the activation mechanism. *Cell*. 2009;137(2):216–233.
14. Del Monte G, Grego-Bessa J, Gonzalez-Rajal A, Bolos V, De La Pompa JL. Monitoring Notch1 activity in development: Evidence for a feedback regulatory loop. *Dev Dyn*. 2007;236(9):2594–2614.
15. Kokubo H, et al. Targeted disruption of hesr2 results in atrioventricular valve anomalies that lead to heart dysfunction. *Circ Res*. 2004;95(5):540–547.
16. Kokubo H, Miyagawa-Tomita S, Nakazawa M, Saga Y, Johnson RL. Mouse hesr1 and hesr2 genes are redundantly required to mediate Notch signaling in the developing cardiovascular system. *Dev Biol*. 2005;278(2):301–309.
17. Fischer A, et al. Combined loss of Hey1 and HeyL causes congenital heart defects because of impaired epithelial to mesenchymal transition. *Circ Res*. 2007;100(6):856–863.
18. Beis D, et al. Genetic and cellular analyses of zebrafish atrioventricular cushion and valve development. *Development*. 2005;132(18):4193–4204.
19. Watanabe Y, et al. Activation of Notch1 signaling in cardiogenic mesoderm induces abnormal heart morphogenesis in mouse. *Development*. 2006; 133(9):1625–1634.
20. Murtaugh LC, Stanger BZ, Kwan KM, Melton DA. Notch signaling controls multiple steps of pancreatic differentiation. *Proc Natl Acad Sci U S A*. 2003;100(25):14920–14925.
21. Kisanuki YY, Hammer RE, Miyazaki J, Williams SC, Richardson JA, Yanagisawa M. Tie2-Cre transgenic mice: a new model for endothelial cell-lineage analysis in vivo. *Dev Biol*. 2001;230(2):230–242.
22. Nakagawa O, Nakagawa M, Richardson JA, Olson EN, Srivastava D. HRT1, HRT2, and HRT3: a new subclass of bHLH transcription factors marking specific cardiac, somitic, and pharyngeal arch segments. *Dev Biol*. 1999;216(1):72–84.
23. Krebs LT, et al. Notch signaling is essential for vascular morphogenesis in mice. *Genes Dev*. 2000;14(11):1343–1352.
24. Lamar E, et al. Nrarp is a novel intracellular component of the Notch signaling pathway. *Genes Dev*. 2001;15(15):1885–1899.
25. Palomero T, et al. NOTCH1 directly regulates c-MYC and activates a feed-forward-loop transcriptional network promoting leukemic cell growth. *Proc Natl Acad Sci U S A*. 2006;103(48):18261–18266.
26. Zeller R, Bloch KD, Williams BS, Arceci RJ, Seidman CE. Localized expression of the atrial natriuretic factor gene during cardiac embryogenesis. *Genes Dev*. 1987;1(7):693–698.
27. Palmer S, et al. The small muscle-specific protein Csl modifies cell shape and promotes myocyte fusion in an insulin-like growth factor 1-dependent manner. *J Cell Biol*. 2001;153(5):985–998.
28. Christoffels VM, Keijser AG, Houweling AC, Clout DE, Moorman AF. Patterning the embryonic heart: identification of five mouse Iroquois homeobox genes in the developing heart. *Dev Biol*. 2000;224(2):263–274.
29. Jamora C, et al. A signaling pathway involving TGF-beta2 and snail in hair follicle morphogenesis. *PLoS Biol*. 2005;3(1):e11.
30. Akiyama H, et al. Essential role of Sox9 in the pathway that controls formation of cardiac valves and septa. *Proc Natl Acad Sci U S A*. 2004;101(17):6502–6507.
31. Niessen K, Fu Y, Chang L, Hoodless PA, McFadden D, Karsan A. Slug is a direct Notch target required for initiation of cardiac cushion cellularization. *J Cell Biol*. 2008;182(2):315–325.
32. Ansieau S, et al. Induction of EMT by twist proteins as a collateral effect of tumor-promoting inactivation of premature senescence. *Cancer Cell*. 2008;14(1):79–89.
33. Kim RY, Robertson EJ, Solloway MJ. Bmp6 and Bmp7 are required for cushion formation and septation in the developing mouse heart. *Dev Biol*. 2001;235(2):449–466.
34. Camenisch TD, et al. Disruption of hyaluronan synthase-2 abrogates normal cardiac morphogenesis and hyaluronan-mediated transformation of epithelium to mesenchyme. *J Clin Invest*. 2000;106(3):349–360.
35. Liu H, et al. Roles of Chemokine Receptor 4 (CXCR4) and Chemokine Ligand 12 (CXCL12) in Metastasis of Hepatocellular Carcinoma Cells. *Cell Mol Immunol*. 2008;5(5):373–378.
36. Runyan RB, Markwald RR. Invasion of mesenchyme into three-dimensional collagen gels: a regional and temporal analysis of interaction in embryonic heart tissue. *Dev Biol*. 1983;95(1):108–114.
37. Kruzynska-Frejtag A, Machnicki M, Rogers R, Markwald RR, Conway SJ. Periostin (an osteoblast-specific factor) is expressed within the embryonic mouse heart during valve formation. *Mech Dev*. 2001;103(1–2):183–188.
38. Romano LA, Runyan RB. Slug is an essential target of TGFbeta2 signaling in the developing chicken heart. *Dev Biol*. 2000;223(1):91–102.
39. Aybar MJ, Nieto MA, Mayor R. Snail precedes slug in the genetic cascade required for the specification and migration of the Xenopus neural crest. *Development*. 2003;130(3):483–494.
40. Wang Y, et al. Ephrin-B2 controls VEGF-induced angiogenesis and lymphangiogenesis. *Nature*. 2010;465(7297):483–486.
41. Dovey HF, et al. Functional gamma-secretase inhibitors reduce beta-amyloid peptide levels in brain. *J Neurochem*. 2001;76(1):173–181.
42. Rutenberg JB, Fischer A, Jia H, Gessler M, Zhong TP, Mercola M. Developmental patterning of the cardiac atrioventricular canal by Notch and

Hairy-related transcription factors. *Development*. 2006;133(21):4381–4390.
43. Kokubo H, Tomita-Miyagawa S, Hamada Y, Saga Y. Hesr1 and Hesr2 regulate atrioventricular boundary formation in the developing heart through the repression of Tbx2. *Development*. 2007;134(4):747–755.
44. Stanley EG, et al. Efficient Cre-mediated deletion in cardiac progenitor cells conferred by a 3'UTR-ires-Cre allele of the homeobox gene Nkx2-5. *Int J Dev Biol*. 2002;46(4):431–439.
45. Jiao K, et al. An essential role of Bmp4 in the atrioventricular septation of the mouse heart. *Genes Dev*. 2003;17(19):2362–2367.
46. Zhou BP, et al. Dual regulation of Snail by GSK-3beta-mediated phosphorylation in control of epithelial-mesenchymal transition. *Nat Cell Biol*. 2004;6(10):931–940.
47. de Jesus Perez VA, et al. Bone morphogenetic protein 2 induces pulmonary angiogenesis via Wnt-beta-catenin and Wnt-RhoA-Rac1 pathways. *J Cell Biol*. 2009;184(1):83–99.
48. Bachelder RE, Yoon SO, Franci C, de Herreros AG, Mercurio AM. Glycogen synthase kinase-3 is an endogenous inhibitor of Snail transcription: implications for the epithelial-mesenchymal transition. *J Cell Biol*. 2005;168(1):29–33.
49. Tsuji K, et al. BMP2 activity, although dispensable for bone formation, is required for the initiation of fracture healing. *Nat Genet*. 2006;38(12):1424–1429.
50. Sahlgren C, Gustafsson MV, Jin S, Poellinger L, Lendahl U. Notch signaling mediates hypoxia-induced tumor cell migration and invasion. *Proc Natl Acad Sci U S A*. 2008;105(17):6392–6397.
51. Venkatesh DA, Park KS, Harrington A, Miceli-Libby L, Yoon JK, Liaw L. Cardiovascular and hematopoietic defects associated with Notch1 activation in embryonic Tie2-expressing populations. *Circ Res*. 2008;103(4):423–431.
52. Grego-Bessa J, et al. Notch signaling is essential for ventricular chamber development. *Dev Cell*. 2007;12(3):415–429.
53. Hoffman JI, Kaplan S. The incidence of congenital heart disease. *J Am Coll Cardiol*. 2002; 39(12):1890–1900.
54. Ii M, et al. Notch signaling regulates endothelial progenitor cell activity during recovery from arterial injury in hypercholesterolemic mice. *Circulation*. 2010;121(9):1104–1112.
55. Oka C, et al. Disruption of the mouse RBP-J kappa gene results in early embryonic death. *Development*. 1995;121(10):3291–3301.
56. Salmon P, Trono D. Production and titration of lentiviral vectors. *Curr Protoc Neurosci*. 2006; Chapter 4:Unit 4.21.